SYNTHESIS, CHARACTERIZATION, AND LUMINESCENT PROPERTIES OF Eu^{3+} DIPYRIDOPHENAZINE FUNCTIONALIZED COMPLEXES FOR POTENTIAL BIO-IMAGING APPLICATIONS

A Thesis

Presented to the faculty of the Graduate School of
Western Carolina University in partial fulfillment of the
requirements for the degree of Master of Science in Chemistry.

By

Jeremy Beasley

Advisor: Dr. Brian Dinkelmeyer,
Associate Professor, Organic Chemistry,
Department of Chemistry & Physics

Committee Members: Dr. Channa De Silva, Chemistry
Dr. David Evanoff, Chemistry

October 2014

ACKNOWLEDGEMENTS

I would like to thank my research committee for all of their guidance, and in particular Dr. Brian Dinkelmeyer. You were more help than you give yourself credit for, and thank you for the opportunity. I would also like to thank Will Reece for his contributions to my project, my family for their support, and my future wife for her ability to put up with me on a daily basis ☺.

TABLE OF CONTENTS

LIST OF TABLES

LIST OF FIGURES

LIST OF SCHEMES

LIST OF ABBREVIATIONS

ATR	Attenuated total reflectance
APTS	3-aminopropyltriethoxysilane
DPPZ	Dipyrido[3,2-a:2',3'-c]phenazine
DPPZ-COOEt	Dipyrido[3,2-a:2',3'-c]phenazine-11-ethyl ester
DPPZ-CH_3	Dipyrido[3,2-a:2',3'-c]phenazine-11-methyl
DPPZ-COOH	Dipyrido[3,2-a:2',3'-c]phenazine-11-carboxylic acid
DPPZ-Si	Dipyrido[3,2-a:2',3'-c]phenazine-11-carboxamide,N-[3-(triethoxysilyl)propyl]
FTIR	Fourier transform infrared spectroscopy
NMR	Nuclear magnetic resonance spectroscopy
UV-Vis	Ultraviolet-Visible absorption spectroscopy
tta	2-thenoyltrifluoroacetone

ABSTRACT

SYNTHESIS, CHARACTERIZATION, AND LUMINESCENT PROPERTIES OF EU^{3+} DIPYRIDOPHENAZINE FUNCTIONALIZED COMPLEXES FOR POTENTIAL BIO-IMAGING APPLICATIONS.

Jeremy Beasley

Western Carolina University (November 2014)

Director: Dr. Brian Dinkelmeyer

Luminescent properties of lanthanide complexes possess unique characteristics that make them good candidates for possible bioimaging agents and have inspired research initiatives to further explore these materials. However, the toxicity of these metals limits their applications as *in-vivo* bioimaging agents. One solution that eliminates the toxic effects is to encase these lanthanide complexes in silica. This project was designed to probe the variation in the fluorescence properties of a highly luminescent europium (III) complex, utilizing a fluorinated β-diketonate ligand (thenoyltrifluoroacetone (tta)), upon the substitution of the solvent molecules by various functionalized dipyrido[3,2-a:2',3'-c]phenazine (DPPZ) ligands. A method for covalently attaching, or occluding complexes in silica nanoparticles were also included in the project design. The structure and properties of the functionalized DPPZ ligands and their respective complexes were determined by FT-IR, ^{1}H-NMR, UV-Vis, and fluorescence spectroscopy techniques. UV excitation of the complexes resulted in red luminescence (~ 614 nm) characteristic of trivalent europium ions. The differences in luminescence properties of the complexes are rationalized in terms of the electronic features of the different functionalized DPPZ ligands. The higher overall quantum yield of the un-functionalized DPPZ complex, $Eu(tta)_3DPPZ$ (Q.Y.= 7.68 ± 0.06 %), and the low overall quantum yield observed for $Eu(tta)_3DPPZ$-COOEt (Q.Y.= 1.08 ± 0.05%), $Eu(tta)_3DPPZ$-Si (Q.Y.= 0.65± 0.04%),

$Eu(tta)_3DPPZ$-COOH (Q.Y.= 0.61± 0.07 %), $Eu(tta)_3DPPZ$-CH_3 (Q.Y.= 0.59±0.02 %) are rationalized in terms of how electron donating or withdrawing groups affect their respective ligand-to-metal energy transfer efficiencies. $Eu(tta)_3DPPZ$ was the only complex to show enhanced luminescent properties capable of potential applications in biomedical imaging.

CHAPTER 1: INTRODUCTION

1.1 Problem Statement

Inorganic-organic hybrid materials are an emerging class of materials whose properties can be tailored depending on the application. In particular, luminescent nanomaterials whose areas of application range from optics and electronics to energy, environment, biology and medicine. More specific applications include photovoltaic cells, micro-optical/-electronic components, nanophotonics, cosmetics, light emitting diodes, laser technology, as well as controlled targeting and release of active molecules for medical imaging and therapy purposes.[4,7]

Inorganic sol-gel materials have been the focus of recent research due to their attractive photonic capabilities as well as their low cost in developing siloxane based matrices. Research in this area includes light emitting lanthanide-based multi-functional hybrids with potential applications in tunable lasers, amplifiers for optical communications, emitter layers in multilayer light emitting diodes, efficient light conversion molecular devices, and light concentrators for photovoltaic devices.[1,2,5] A significant part of this research has involved the encapsulation of lanthanide organic complexes with diketonates, aromatic carboxylic acids, or heterocyclic ligands into hybrid matrices through (i) simple embedding of the complexes,[10-12] (ii) use of ligands covalently grafted to the framework,[10,21] or (iii) anchoring the metal center to specific functional groups of the hybrid matrix.[22-31] Some of these works explicitly quantified the modifications in the emission features of the hybrids, relative to those of the precursor complex. There was an improvement in the photostability under UV radiation (one of the drawbacks of lanthanide diketonate chelates) and the increase in the emission quantum yields relative to their

corresponding precursor complexes.[10] Lanthanide ions exhibit limited photo-bleaching, higher chemical stability which make them more sought after alternatives to organic dyes.[7]

1.2 Background

1.2.1 Lanthanide and Ligand Chemistry

The properties that make lanthanide complexes of particular interest are their long luminescence lifetimes and narrow emission bands.[1-2,4-5] These characteristics make them good candidates for possible bio-imaging agents. The 4*f* orbitals of lanthanide (III) ions are shielded by the filled 5*s* and 5*p* sub-shells, which are the source of their narrow emission bands. Lanthanide (III) ion's 4*f*-4*f* electronic transitions are forbidden by the electric dipole selection rules due to their orbital parity (Laporte forbidden) being the same in both the initial and final electronic states. This makes direct excitation of f-electrons from lanthanide (III) ions difficult to reach an emissive level. The selection rules are conducive to the lanthanide (III) ion's being excited either during a temporary change in geometric arrangement around the ion, or mixing with opposite parity wave functions from 5d orbitals, ligand orbitals, or charge transfer states.[1] Because the likelihood of an electric dipole f-f transition is low and direct excitation of a lanthanide (III) ion is difficult, an organic chromophore (antenna) ligand can be used to transfer energy to the lanthanide (III) ion. The ligands are covalently bound to the lanthanide and transfer energy through a process described as "the antenna effect".[1] The ligands (antennae) are capable of absorbing light, and transferring the energy of that light to the lanthanide (III) ion.

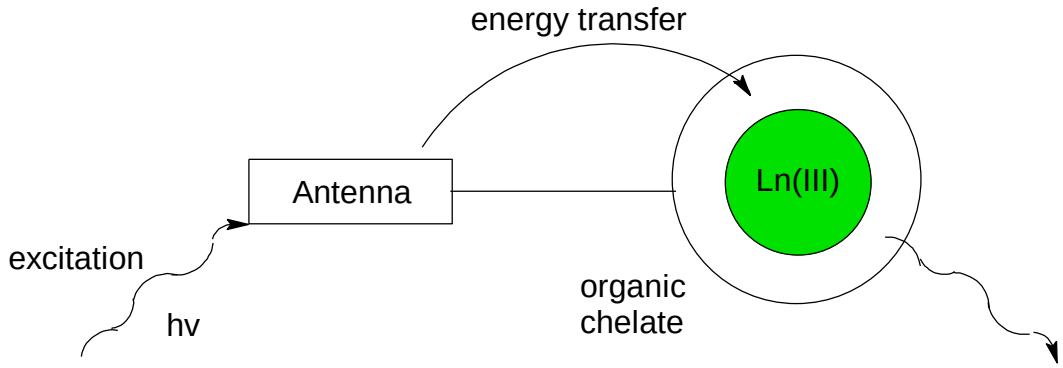

Figure 1. An illustration of the "antenna" effect, where incident excitation is absorbed by a chelating organic chromophore and energy is transferred to the metal.

Excitation of the ligand causes electrons to eventually inhabit the triplet state of the ligand (by intersystem crossing). From there electrons can transfer energy from the triplet state to the emissive state of the lanthanide complex center. For the sensitization of the lanthanide (III) ion to be more efficient, the antenna ligand needs to have a triplet state (T_1) energy similar to that of the energy of the lanthanide (III) ions in order to achieve an efficient energy transfer necessary for emission of the lanthanide complexes. The structural parameters also play a role in energy transfer as the distance between the antenna and the metal ion is crucial for an efficient energy transfer process.[20]

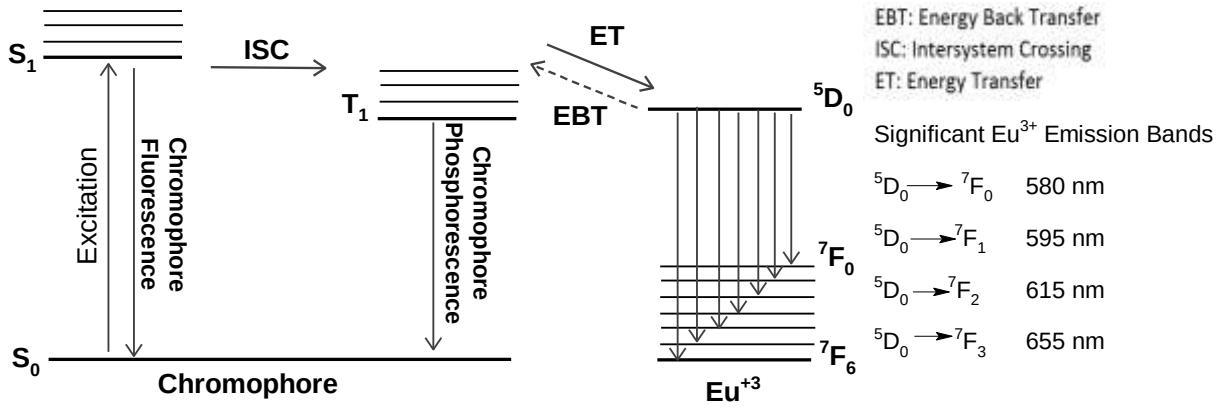

Figure 2. Jablonski diagram showing the energy transfer from the excited state of the ligand to the excited state of the europium ion and to the ground state via luminescence.

Europium (III) complexes with appropriate antenna ligands have many advantages over other lanthanide complexes as bio-imaging agents. The advantage of these Eu^{3+} complexes over other lanthanide complexes is that they can be adequately sensitized with longer wavelength (visible) light which is less harmful to the biological targets (tissues, cells, etc.) than traditional UV excitation.[21] Another advantage of Eu^{3+} complexes is that they have a narrow emission line that occurs in the red light region which have minimal interference from luminescing biological samples.[4] Additionally, Eu^{3+} complexes have a high luminescence quantum yield, large Stokes shift and a long luminescence lifetime on the millisecond order.[1] These properties make Eu^{3+} a prime candidate to coordinate with organic chromophore ligands used in biomedical imaging applications.

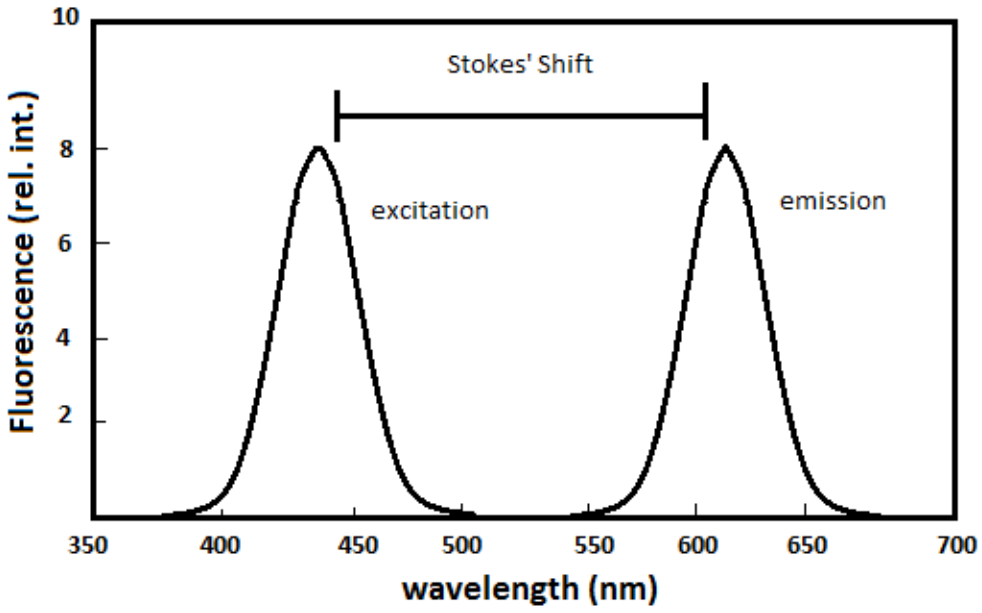

Figure 3. Example spectra demonstrating the Stokes shift.

Modulating/optimizing the luminescent properties of lanthanide ion complexes can be accomplished by systematically varying the identity of their attached ligands.

To get a luminescing organometallic complex for potential bioimaging applications, the appropriate ligand must first be chosen and synthesized. These properties impact the potential

use of these complexes in biomedical applications. More specifically, if used in a bio-imaging application, the biocompatibility of these complexes would have to be determined. Furthermore, if they were found to be toxic, their use would require that these complexes first be rendered harmless. One limitation of lanthanide based bioimaging agents is their toxicity. This toxicity can be mediated by using a silane coupling agent, capable of forming/binding to silica nanoparticles, to functionalize the ligand coordinating to the Eu^{3+} complex in order to make it a more biocompatible matrix.[6,11-12,15] This offers only a partial solution since the porosity of glass may allow Eu^{3+} to diffuse out of the Si-glass matrix, and into the biological sample.

An organic photoactive chelator, usually in the form of a multi-dentate ligand with an appropriate chromophoric antenna attached is chosen. Coordination with monodentate ligands are typically weak, and they are unable to adequately displace water molecules from the first coordination sphere.[3] However, a chelating antenna ligand (in conjunction with other chelating ligands) coordinates to the lanthanide ion, and facilitates energy transfer between the two. This protects the lanthanide from coordination with water (or other solvents), and provides a structure to which other reactive functional groups can be attached.[3]

1.2.2 Silane and Sol-Gel Chemistry

Silane coupling agents have the ability to form durable bonds between organic and inorganic materials. The basic structure for a silane coupling agent typically has two reactive groups. The X (hydrolyzable) group is typically alkoxy, acyloxy, halogen or amine in nature, and reacts with the inorganic portion of the desired substrate. The R group is a nonhydrolyzable organic radical that binds to another organic compound, and may possess a functionality that imparts desired characteristics to that compound.

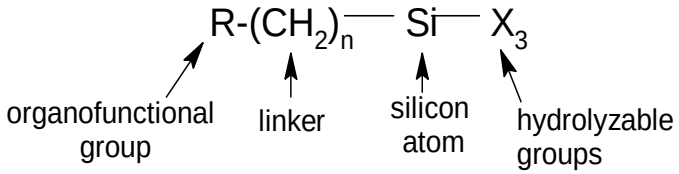

Figure 4. General structure formula for a silane coupling agent.

The most widely used organosilanes have one organic substituent and three hydrolyzable substituents. Maximum hydrolytic stability (resistance to water) can be achieved with three hydrolyzable substituents. Reaction of silanes occurs during four different processes. Firstly, hydrolysis of the three X groups occurs. Secondly, condensation to oligomers follows hydrolysis. Thirdly, the oligomers then hydrogen bond with OH groups of the substrate. Finally, during drying, a covalent bond is formed with the substrate while losing water.[24]

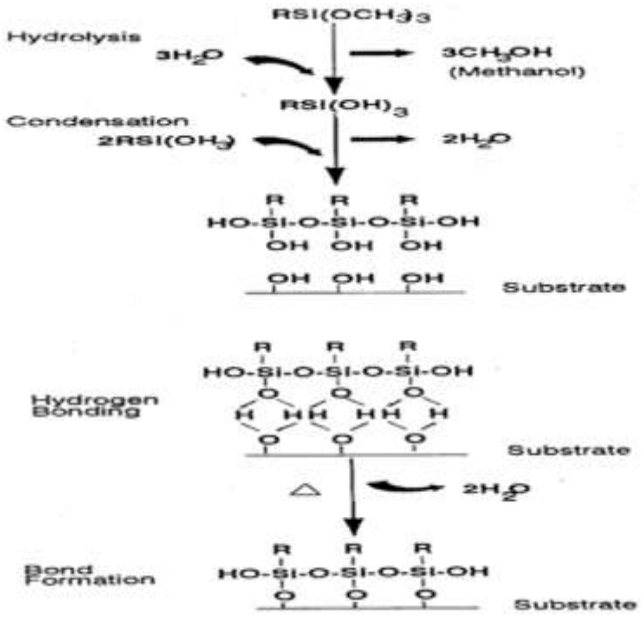

Figure 5. General process for the bond formation of silanes to a substrate.[24]

There is usually only one bond from each silicon of the organosilane to the substrate surface. The R group remains available for covalent reaction with other organic compounds.

The coupling agents linker ($(CH_2)_n$), between the organic functionality and the silicon atom, plays a role in determining what properties the system will have. Depending on the length of the linker a systems physical properties may vary and reactivity inhibited. Many applications, such as sensors, composite and fluorescent materials, require that reactive centers be close in proximity to the substrate in order to maximize the utilization of their desired properties. Steric constraints and the accessibility of the organic functional group near the inorganic surfaces are of concern when designing a system with silane coupling agents. As the linker length increases the organic functional group has the ability to extend further away from the surface of the inorganic substrate. The characteristics of silane coupling agents are of particular importance when designing luminescent materials for biological applications.[24]

1.3 Objectives

The questions and concerns described above, are the basis from which this research project was designed. The goal of this project was to synthesize functionalized phenanthroline-based ligands, coordinate them to Eu^{3+}, to investigate their absorbance and fluorescence properties, study the variation in complex luminescence upon substituent substitution of the ligand, and develop a method for covalently attaching or occluding them in silica nanoparticle. Having the europium complexes covalently bound within a silica matrix will minimize any diffusion of these complexes out of the glass and preclude any toxicity effects. Sol-gel derived siloxane hybrid materials have attracted interest for their possible photonic applications due to their ability to combine the optical quality of silica, along with its thermal stability and mechanical strength, with the characteristics of organic molecules (chromophores). Organic chelates are known to be adequate sensitizers of lanthanide ions. Organic chelates also help reduce the hydroxyl concentrations and quenching during the formation of the siloxane matrixes.

Dipyridophenazine (DPPZ) was chosen as the appropriate phenanthroline-based ligand for this project.

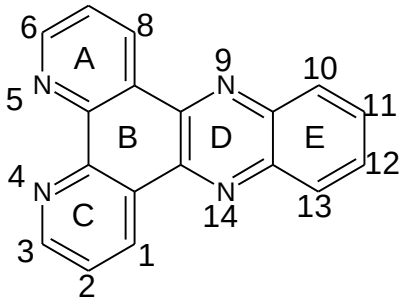

Figure 6. Structure of DPPZ with ring labels and numbering.

DPPZ is an organic, chelating (bidentate) ligand that is planar, chromophoric, heterocyclic, and aromatic in nature. Metal complexes which contain these DPPZ ligands have been shown to intercalate with DNA. This allows for non-covalent insertion of the aromatic rings between the base pairs in the DNA double helix via electrostatic and van der Waals forces, which eventually lengthens, stiffens and unwinds the double helix.[3,7] This makes intercalators sought after mutagens that inhibit transcription, replication and other DNA repair processes implemented in anti-cancer agents. The study of the intercalating behavior in DNA processes are beyond the scope this project, and will not be examined.

DPPZ is also a compound of interest because of its electronic structure. Reduction of these ligands leads to the formation of radical anion with a charge located on the phenazine part of the ligand. Unoccupied molecular orbitals (MO's) are located over either the phenanthroline (phen; rings A, B and C), or the phenazine (phz; rings B, D and E) portions of the ligand. The molecular orbital model used to describe the properties of DPPZ was probed in a series of experiments.[13] Through substitution of functional groups to DPPZ it is possible to tune the energy level of the phz portion of the ligand. Substituting electron withdrawing groups leads to a

more positive reduction potential, while substituting electron donating groups results in a more negative reduction potential. The more negative the reduction potential the higher the electron transfer potential becomes.[9]

This project focused on investigating the structural and electronic effects of unsubstituted DPPZ as well as substituting a methyl, carboxylic acid, ethyl ester and amidosilane at the 11 position of DPPZ. Thenoyltrifluoracetone (tta) was coordinated to three bidentate sites (six total coordination sites) of the europium (III) coordination complex to boost the luminescence efficiency of the complexes due to β-diketonates being very efficient chromophores. The effects of coordinating the functionalized DPPZ ligands to the europium (III) coordination complex via the displacement of two water molecules were monitored.

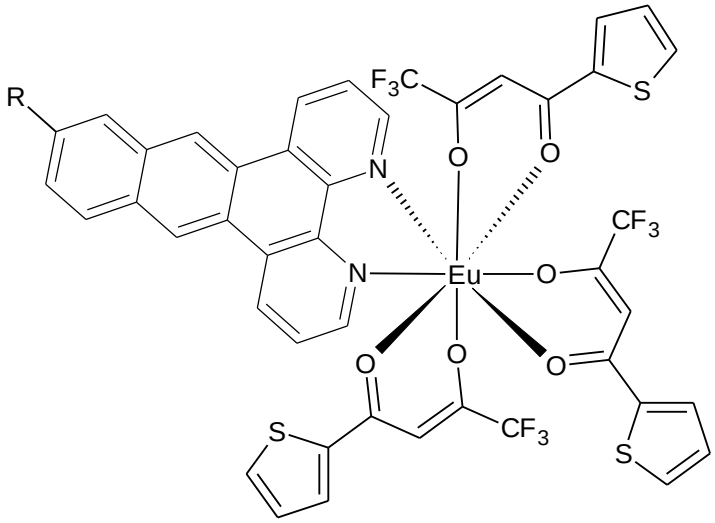

Figure 7. Proposed structure of the octacoordinate europium complex utilizing tta, and functionalized DPPZ ligands. R= -H, -CH_3, -COOH, -COOEt, -Si.

Measuring the effects of occluding the DPPZ-Si coordination complex within a silica nanoparticle was also probed. The synthesis of these ligands, complexes and nanoparticles, and characterization using FTIR and NMR techniques are reported. Due to limited resources their crystal structures were unable to be determined for the ligands and complexes. Electronic

properties of the ligands and their coordination complexes were investigated using UV-Vis absorption spectroscopy and fluorescence spectroscopy. In the future, these results could be used to explore the substituent effects on the complexes using computational methods such as density functional theory (DFT).

CHAPTER 2: EXPERIMENTAL

All reagents were purchased from Sigma Aldrich or Acros Organics and used without further purification unless otherwise stated. Synthesized ligands and complexes were characterized using Fourier-transform infrared spectroscopy (FT-IR), nuclear magnetic resonance (NMR, when applicable), UV-visible and fluorescence spectroscopic techniques. The methods used for characterization will be discussed in this section along with all instrument specifications.

2.1 Materials and Instrumentation

2.1.1 Fourier Transform Infrared Spectroscopy

FTIR spectra were obtained using a Perkin Elmer Spectrum One. All measurements were performed at room temperature with a scanning range of 4000 cm^{-1} – 600 cm^{-1}, using single-bounce attenuated total reflectance with a diamond crystal. For all of the materials that were measured as a solid powder (all solvents had been removed), the background was performed on the instrument room environment. The ATR plate was cleaned with a Kimwipe and acetone between each measurement.

2.1.2 Nuclear Magnetic Resonance Spectroscopy

NMR spectra were obtained using a JEOL 300 MHz Eclipse NMR with a 5 mm probe capable of detecting ^{1}H and ^{13}C nuclei. Proton NMR samples were prepared using ~10 mg of material, in either deuterated chloroform ($CDCl_3$) or deuterated dimethyl sulfoxide (d6-DMSO) unless otherwise stated, and spectra were obtained using a varying number of scans ranging from 16-128 as to ensure an adequate signal-to-noise ratio was acquired. Carbon NMR samples were prepared similarly, except material was added until the deuterated solution became saturated.

2.1.3 UV-Visible Absorption Spectroscopy

UV-Vis spectra were collected using an Agilent 8453 UV-Vis spectrometer at room temperature. This instrument has two different sources: a deuterium lamp (for UV measurements), and a tungsten lamp (for visible measurements). The use of a photodiode array detector allows the spectrometer to detect a wavelength range of 190 nm – 1100 nm at 1 nm intervals. All of the blank and sample measurements were made using a quartz cuvette (1 cm path length). There were three different solvents used to dissolve the ligands and their respective complexes: chloroform (DPPZ-COOEt, DPPZ-Si, $Eu(tta)_3(H_2O)_2$, $Eu(tta)_3$DPPZ-COOEt, and $Eu(tta)_3$DPPZ-Si), dimethyl sulfoxide (DPPZ-CH_3, DPPZ-COOH, $Eu(tta)_3$DPPZ-CH_3, and $Eu(tta)_3$DPPZ-COOH), and acetonitrile (DPPZ, and $Eu(tta)_3$DPPZ). Blanks were obtained of the solvent, and all samples dissolved in that particular solvent were subsequently measured to prevent the need for continuous re-blanking. For the quantum yield measurements, analytical grade solvents were used and cresyl violet was used as the reference material. The cresyl violet was dissolved in methanol, a blank containing methanol was used for those measurements. All of the samples of interest, as well as the reference samples, that were prepared for the quantum yield measurements were adjusted to have absorbance values less than 0.1 A.U. Each sample was measured in triplicate on three different days, and all the spectra were averaged in order to account for any possible environmental or instrumental error associated with the measurements.

2.1.4 Fluorescence Spectroscopy

Fluorescence spectra were acquired using a Perkin Elmer LS-55 Luminescence Spectrometer at room temperature. The same solvent systems for the blanks (to correct for any solvent fluorescence), samples and references that were used for UV-Vis measurements were also used for fluorescence measurements. A quartz cuvette was used for all measurements. A

scanning range of 200 nm – 800 nm with a scan speed of 200 nm/min was used, with an excitation and emission slit of 5.0 nm.

2.1.5 Quantum Yield Measurements

The quantum yield calculations were made using the ae UV-Vis-IR Spectral Software by FluorTools.[25] The software utilizes the following equation:

$$QY = QY_{ref}\left(\frac{n^2}{n_{ref}^2}\right)\left(\frac{I}{A}\right)\left(\frac{A_{ref}}{I_{ref}}\right)$$

where QY is the quantum yield of the compound, n is the refractive index of the solvent, I is the integrated fluorescence intensity and A is the absorbance at the excitation wavelength. Cresyl violet (QY=0.54) was chosen as the reference compound, and was prepared in methanol (n=1.3284). The excitation wavelength for cresyl violet was at 592 nm (A=0.06006), while the emission range used to calculate the integrated fluorescence intensity (I=21608.99) for cresyl violet was from 550-725 nm. These values remain the same for the quantum yield calculations for all of the complexes.

For the Eu^{3+} complexes a variety of solvents were utilized. $Eu(tta)_3DPPZ$, $Eu(tta)_3DPPZ$-CH_3/$Eu(tta)_3DPPZ$-COOH, and $Eu(tta)_3DPPZ$-COOEt/$Eu(tta)_3DPPZ$-Si measurements were made in acetonitrile (n=1.3441), DMSO (n=1.4793), and chloroform (n=1.4458) respectively. The excitation wavelength ranges from 342-349 nm for the various complexes, while the emission range used to calculate the integrated fluorescence intensity for the complexes was from 550-664 nm. Baseline absorption and emission spectra of pure solvents were also collected (at their respective excitation wavelengths) to be subtracted from the measured absorption and emission spectra to correct for background absorption or emission imparted by the solvents. Each sample was measured in triplicate on three different days, and all the spectra were averaged

in order to account for any possible environmental or instrumental error associated with the measurements.

2.2 Functionalized Dipyridophenazine Ligand Preparation

2.2.1 Synthesis of 1,10-phenanthroline-5,6-dione[8]

1,10-phenanthroline-5,6-dione was synthesized from one equivalent of 1,10-phenanthroline (fw:198.23 g/mol, 1.164g, 0.008587 mol), 2.5 equivalents of potassium bromide (fw:119.01 g/mol, 2.4889 g, 0.02091 mol,), 37.5 equivalents of sulfuric acid (d=1.84 g/mL;16.6 mL, 0.312 mol), and 15 equivalents of nitric acid (d=1.42 g/mL;8.00 mL, 0.126 mol). Sulfuric and nitric acid were added dropwise to the round bottom flask containing the dione and potassium bromide. Orange bromine gas begins to form and is continually purged with argon. The reaction was heated at reflux until the formation of bromine gas dissipated. The solution was poured into an ice bath and brought to a neutral pH using 6M sodium hydroxide to form a yellow solution. The solution was extracted with dichloromethane and dried with magnesium sulfate. The solution was then filtered to remove the magnesium sulfate and rotovapped, yielding a yellow solid product. The crude product was dissolved in chloroform, and recrystallized from chloroform to hexanes. Yield: 4.4 g (84 %). ^{1}H-NMR ($CDCl_3$, 300MHz): δ 9.06 (d, 2H), 8.44 (d, 2H), 7.55 (dd, 2H) ppm. FTIR (ATR): 1718, 1687 cm^{-1}.

2.2.2 Synthesis of Dipyrido[3,2-a:2',3'-c]phenazine (DPPZ)[17]

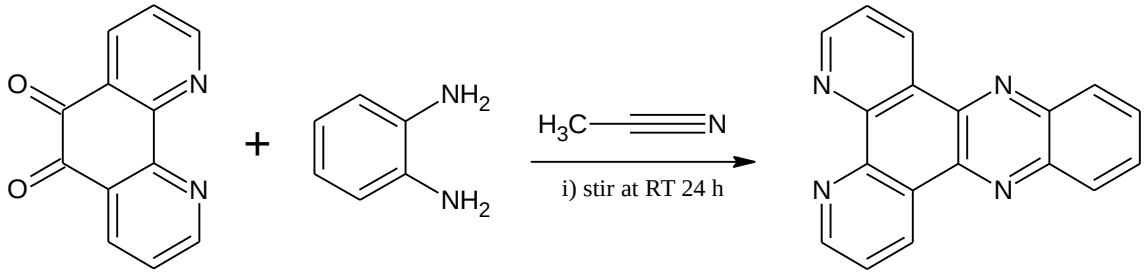

Scheme 1. Reaction scheme for dipyrido[3,2-a:2',3'-c]phenazine (DPPZ).

DPPZ was synthesized from one equivalent of 1,10-phenanthroline-5,6-dione (fw: 210.19 g/mol, 0.1171 g, 0.557 mmol) and one equivalent of o-phenylene diamine (fw: 108.14 g/mol, 0.0614 g, 0.568 mmol). Dichloromethane (6.00 mL) was added and allowed to stir until most of the starting material had gone into solution before acetonitrile (2.65 mL) was added. The solution was allowed to stir for 24 hours, and rotovapped to give final product. No further purification was done. Yield: 0.116 g (76%). ^{1}H-NMR (d_6-DMSO, 300MHz): δ 9.54 (dd, 2H), 9.23 (dd, 2H), 8.41 (dd, 2H), 8.09 (dd, 2H), 7.93 (dd, 2H) ppm. FTIR (ATR): 2943, 1480, 819, 737 cm^{-1}. UV/vis (CH_3CN): λ_{max} = 268 nm, 359 nm, 378 nm. Fluorescence (CH_3CN, λ_{ex} = 386 nm): λ_{em} = 432 nm.

2.2.3 Synthesis of Dipyrido[3,2-a:2',3'-c]phenazine-11-methyl (DPPZ-CH_3)

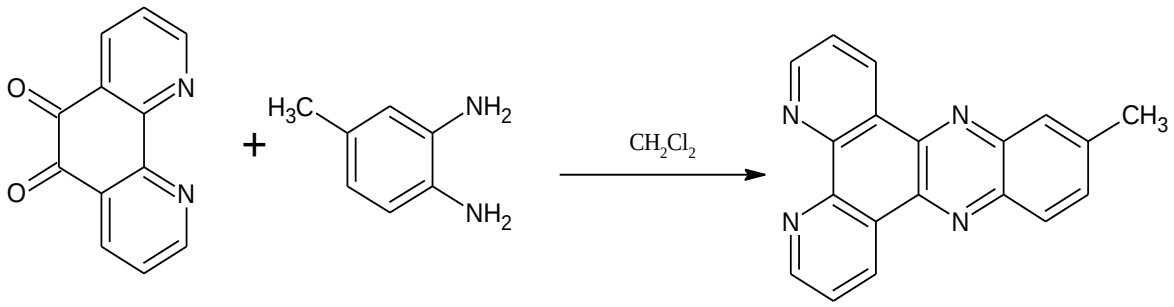

Scheme 2. Reaction scheme for *dipyrido[3,2-a:2',3'-c]phenazine-11-methyl (DPPZ-CH_3).*

1,10-phenanthroline-3,4-diaminotoluene was synthesized from one equivalent of 1,10-phenanthroline-5,6-dione (fw: 210.19 g/mol, 0.2275 g, 1.08 mmol), and one equivalent of 3,4-diaminotoluene (fw: 122.17 g/mol, 0.1329 g, 1.09 mmol) in dichloromethane. First, the dione was dissolved in dichloromethane (5 mL) before diaminotoluene was added. The solution was gently heated overnight. The solvent evaporated overnight. Chloroform was added to the product and dissolved. Recrystallization from chloroform to hexanes yielded small red crystals. No further purification was performed. ^{1}H-NMR ($CDCl_3$, 300MHz): δ 9.70 (dd, 2H), 9.36 (d, 2H), 8.19 (dd, 2H), 7.88 (dd, 2H), 7.80 (dd, 1H), 2.73 (s, 3H) ppm. FTIR (ATR): 2943, 1480,

819, 737 cm^{-1}. UV/vis (DMSO): λ_{max} = 273 nm, 367 nm, 387 nm. Fluorescence (DMSO, λ_{ex} = 330 nm): λ_{em} = 413 nm.

2.2.4 Synthesis of Ethyl 3,4-diaminobenzoate

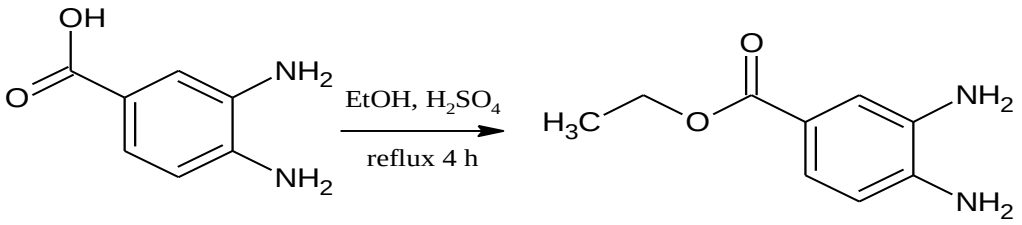

Scheme 3. Reaction scheme for ethyl-3,4-diaminobenzoate.

3,4-diaminobenzoic acid (fw: 152.15 g/mol, 1.5090 g, 9.92 mmol) was dissolved in boiling ethanol (EtOH, 90 mL). Concentrated sulfuric acid (3 mL) was added dropwise to the solution, and heated at reflux for four hours. Solvent was then removed under vacuum. Crude product was dissolved in water (~60 mL), and the pH was adjusted to 10 via addition of 3M NaOH. The aqueous layer was extracted by multiple washes with $CHCl_3$, and washing of the organic layer with brine and water, evaporation of chloroform yielded a yellow solid product. No further purification was performed. The product was dissolved in EtOH (~120 mL) and refrigerated, to prevent possible polymerization of the product. No further characterization was performed because of this being an intermediate. Yield: 1.57 (86 %) ^{1}H-NMR: (D_2O, 300MHz): δ 7.67 (m, 2H), 7.07 (d, 1H), 4.559 (qt, 2H), 1.598 (t, 3H).

2.2.5 Synthesis of Dipyrido[3,2-a:2',3'-c]phenazine-11-ethyl ester (DPPZ-COOEt)

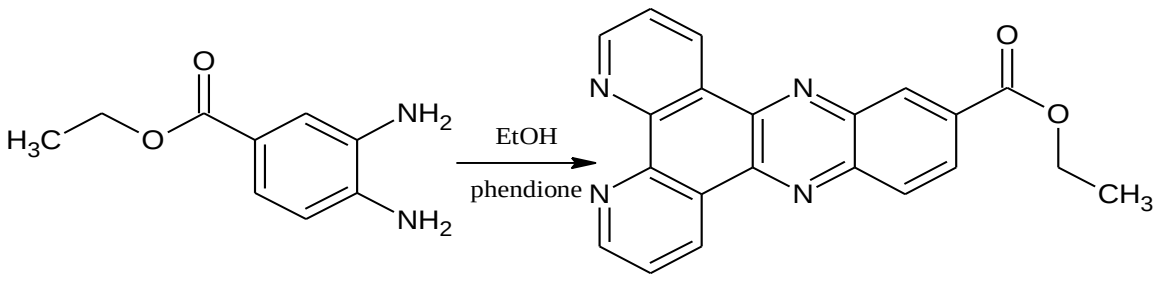

Scheme 4. Reaction scheme for dipyrido[3,2-a:2',3'-c]phenazine-11-ethyl ester (DPPZ-COOEt).

One equivalent of 1,10-phenanthroline-5,6-dione (fw: 210.19 g/mol, 0.3647 g, 1.74 mmol) was added to EtOH (15 mL) and $CHCl_3$ was added until solid dissolved. Once dissolved, one equivalent of ethyl 3,4-diaminobenzoate-EtOH solution (30 mL, 0.33 g, 1.83 mmol) was added dropwise to the boiling solution. A brownish tan precipitate was formed during the mixing. The mixture was heated at reflux for ~30 minutes. Crude product was collected via vacuum filtration. Solid product was recrystallized from chloroform to hexanes. Yield: 0.380 g (82 %). ^{1}H-NMR ($CDCl_3$, 300MHz): δ 9.65 (dd, 2H), 9.31 (dd, 2H), 9.09 (d, 1H), 8.47(dddd, 2H), 7.84 (dd, 2H), 4.55 (qt, 2H), 1.52 (t, 3H) ppm. FTIR (ATR): 3016, 2943, 1711,1406 1204, 738 cm^{-1}. UV/vis ($CHCl_3$): λ_{max} = 277 nm, 366 nm, 386 nm. Fluorescence ($CHCl_3$, λ_{ex} = 386 nm): λ_{em} = 435 nm.

2.2.6 Synthesis of Dipyrido[3,2-a:2',3'-c]phenazine-11-carboxylic acid (DPPZ-COOH)

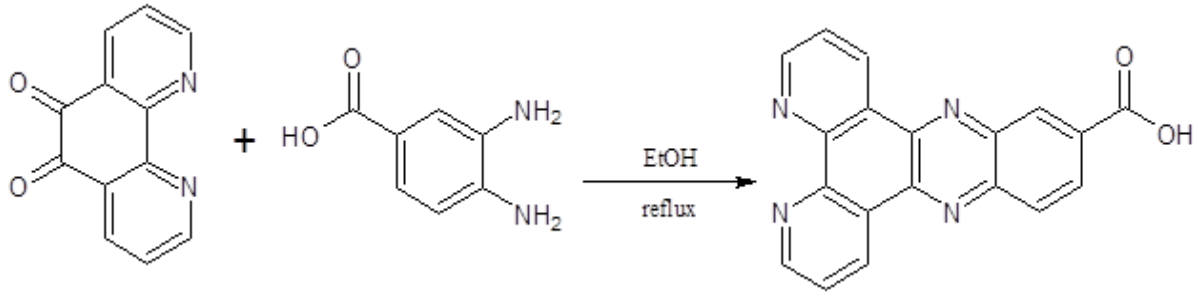

Scheme 5. Reaction scheme for dipyrido[3,2-a:2',3'-c]phenazine-11-carboxylic acid (DPPZ-COOH).

Method a. The synthesis of the carboxylic acid functionalized dppz was synthesized from one equivalent of 1,10-phenanthroline-5,6-dione (fw: 210.19 g/mol, 0.1534 g, 0.730 mmol) with one equivalent of 3,4-diaminobenzoic acid (fw: 152.15 g/mol, 0.1110 g, 0.730 mmol). 1,10-phenanthroline-5,6-dione was added to boiling EtOH (~20 mL) and $CHCl_3$ was added until solid dissolved, and 3,4-diaminobenzoic acid was dissolved in boiling EtOH (~10 mL). Once both solutions had completely dissolved the starting materials, the solutions are mixed together and heated at reflux for 10 minutes. A greyish tan precipitate began to form. After cooling, the

precipitate was vacuum filtered and washed with ethanol to remove impurities and dried under vacuum. The crude product consisted of a mixture of starting material and product that was difficult to separate. Yield: 0.298 g (81 %). H^1 NMR (d_6-DMSO, 300MHz): δ 9.58 (dd, 2H), 9.24 (dd, 2H), 8.84 (d, 1H), 8.50 (dd, 2H), 8.08 (dd, 2H), 3.45 (s, 1H) ppm. FTIR (ATR): 3345, 3050, 2945, 1727, 1089, 1045, 724 cm^{-1}.

Method b. The syntheisis of DPPZ-COOH was synthesized by base hydrolosis of DPPZ-COOEt. DPPZ (.0.2168g, 0.612 mmol) was brought to reflux in 65ml of THF and 10ml water. 6M KOH (1.0 ml, 0.612mmol) was added to the reaction vessel and the reaction was allowed to reflux for 30 minutes. The reaction was allowed to cool and stirred at ambient temperature overnight. The THF was removed by rotary evaporation. The reaction was diluted with 20 ml of water and the pH adjusted to 3 with 2M HCl. The white solid product was isolated by vacuum filtration, rinsed with ethanol and dried under vacuum. The product produced was sufficiently pure for further use. Yield: 0.1744 g (88 %). H^1 NMR (d_6-DMSO, 300MHz): δ 9.58 (dd, 2H), 9.24 (dd, 2H), 8.84 (d, 1H), 8.50 (dd, 2H), 8.08 (dd, 2H), 3.45 (s, 1H) ppm. FTIR (ATR): 3345, 3050, 2945, 1727, 1089, 1045, 724 cm^{-1}. UV/Vis (DMSO): λ_{max} = 275 nm, 369 nm, 388 nm. Fluorescence (DMSO, λ_{ex} = 320 nm): λ_{em} = 521 nm.

2.2.7 Synthesis of Dipyrido[3,2-a:2',3'-c]phenazine-11-carboxamide,N –[3-triethoxy)propyl] (DPPZ-Si)

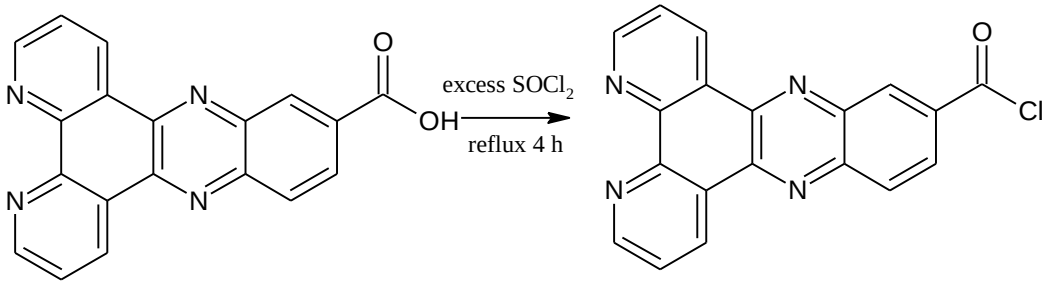

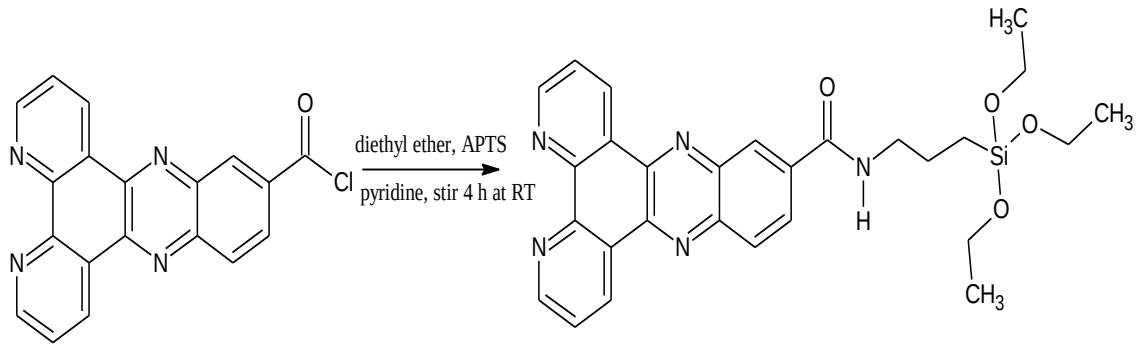

Scheme 6. Reaction scheme for dipyrido[3,2-a:2',3'-c]phenazine-11-carboxamide,N –[3-triethoxy)propyl] (DPPZ-Si).

DPPZ-Si was synthesized via a two-step process. First, DPPZ-COOH (0.1025 g, 0.314 mmol) was dissolved in excess $SOCl_2$ (3 mL) and refluxed for 4 h. The excess $SOCl_2$ was removed under a stream of argon until dry. The tan acid chloride intermediate, DPPZ-COCl (0.1314, 0.381 mmol) was dissolved in anhydrous diethyl ether (15 mL) and placed under inert atmosphere. 3-aminopropyltriethoxysilane (APS= -Si, 0.18 mL, 0.769 mmol) and pyridine (0.07 mL, 0.858 mmol) were mixed in anhydrous diethyl ether (3 mL), and this solution was added dropwise to the DPPZ-COCl mixture. The resulting solution was stirred for 4 h under argon at room temperature. Pyridinium hydrochloride salt precipitate was vacuum filtered out of solution followed by evaporation of diethyl ether and pyridine that led to a red oily residue. Upon further purification, the residue was redissolved in anhydrous diethyl ether and vacuum filtered. The solid product was washed off of the filter paper and dissolved in chloroform. Precipitate that did not dissolve was separated via gravity filtration, and evaporation of solvent at room temperature yielded a clear yellow oil. Yield: 0.873 g (43%). H^1 NMR ($CDCl_3$, 300MHz): δ 9.63 (t, 2H), 9.31 (dd, 2H), 8.71 (d, 1H), 8.38 (dd, 2H), 7.84 (dd, 2H), 3.89 (q, 6H), 3.61 (t, 2H), 1.88 (t, 1H), 1.25 (t, 9H), 0.84 (dd, 4H) ppm. FTIR (ATR): 3274, 3075, 2963, 1640, 1618, 1547, 1099 cm^{-1}. UV/Vis ($CHCl_3$): λ_{max} = 269 nm, 367 nm, 385 nm. Fluorescence ($CHCl_3$, λ_{ex} = 349 nm): λ_{em} = 439 nm.

2.3 Europium Dipyridophenazine Functionalized Complex Preparation

2.3.1 Synthesis of $Eu(tta)_3(H_2O)_2$

Thenoyltrifluoroacetone (tta, 0.7548 g, 3.41 mmol) was added to an aqueous solution of NaOH (0.1342 g, 3.36 mmol in 20 mL H_2O). The solution was allowed to stir for 10 minutes. The resulting clear solution was then added to an aqueous solution of $EuCl_3 \cdot 6H_2O$ (0.4144 g, 1.13 mmol in 12 mL of H_2O) to form a white precipitate, and allowed to stir under nitrogen at 60°C for 30 min and at room temperature for an additional 3 h. The precipitate was filtered off, washed with cold water (2x100 mL), hexane (3 mL) and dried under vacuum for 12 h. Recrystallization of the product from acetone:ethanol (v/v 1:1). The remaining product was dissolved in acetone (30 mL) Yield: 0.3639 g (38 %). UV/vis ($CHCl_3$): λ_{max} = 275 nm, 343 nm. Fluorescence ($CHCl_3$, λ_{ex} = 275 nm): λ_{em} = 614 nm, 594 nm, 580 nm, 652 nm.

2.3.2 Synthesis of $Eu(tta)_3DPPZ$

DPPZ (0.0158 g, 0.056 mmol in 10 mL acetonitrile) was added to a solution of $Eu(tta)_3(H_2O)_2$ (0.0478 g, 0.055 mmol in 4 mL of acetone) and allowed to stir for 30 min at 60°C. Subsequent stirring was done at room temperature for 12 h. The solution was filtered and allowed to evaporate at room temperature yielding the pure product. UV/vis (CH_3CN): λ_{max} = 272 nm, 341 nm, 356 nm, 375 nm. Fluorescence (CH_3CN, λ_{ex} = 342 nm): λ_{em} =613 nm, 592 nm, 580 nm, 652 nm.. Fluorescence quantum yield (λ_{ex}= 342 nm, reference: cresyl violet in MeOH with Φ = 0.54): 7.68 ± 0.06%.

2.3.3 Synthesis of $Eu(tta)_3DPPZ\text{-}CH_3$

DPPZ-CH_3 (0.0137 g, 0.046 mmol in 2 mL DMSO) was added to a solution of $Eu(tta)_3(H_2O)_2$ (0.0437 g, 0.051 mmol in 3.6 mL of acetone) and allowed to stir for 30 min at 60°C. Subsequent stirring was done at room temperature for 12 h. The solution was filtered and allowed to

evaporate at room temperature yielding the pure product. UV/vis (DMSO): λ_{max} = 272 nm, 347 nm, 364 nm, 384 nm. Fluorescence (DMSO, λ_{ex} = 349 nm): λ_{em} = 616 nm , 592 nm, 581 nm, 555 nm, 652 nm. Fluorescence quantum yield (λ_{ex}= 349 nm, reference: cresyl violet in MeOH with Φ = 0.54): 0.59 ± 0.02%.

2.3.4 Synthesis of Eu(tta)$_3$DPPZ-COOH

DPPZ-COOH (0.0241 g, 0.074 mmol in 5 mL DMSO) was added to a solution of $Eu(tta)_3(H_2O)_2$ (0.0630 g, 0.074 mmol in 5.20 mL of acetone) and allowed to stir for 30 min at 60°C. Subsequent stirring was done at room temperature for 12 h. The solution was filtered and allowed to evaporate at room temperature yielding the pure product. UV/vis (DMSO): λ_{max} = 273 nm, 346 nm. Fluorescence (DMSO, λ_{ex} = 349 nm): λ_{em} = 615 nm, 592 nm, 581 nm, 556 nm, 652 nm. Fluorescence quantum yield (λ_{ex}= 349 nm, reference: cresyl violet in MeOH with Φ = 0.54): 0.61± 0.07%.

2.3.5 Synthesis of Eu(tta)$_3$DPPZ-Si

DPPZ-Si (0.0091 g, 0.0171 mmol in 5 mL chloroform) was added to a solution of $Eu(tta)_3(H_2O)_2$ (0.0149 g, 0.0170 mmol in 1.20 mL of acetone) and allowed to stir for 30 min at 60°C. Subsequent stirring was done at room temperature for 12 h. The solution was filtered and allowed to evaporate at room temperature yielding the pure product. UV/vis ($CHCl_3$): λ_{max} = 279 nm, 346 nm, 363 nm, 382 nm. Fluorescence ($CHCl_3$, λ_{ex} = 347 nm): λ_{em} = 613 nm, 592 nm, 580 nm, 652 nm. Fluorescence quantum yield (λ_{ex}= 347 nm, reference: cresyl violet in MeOH with Φ = 0.54): 0.65± 0.04%.

2.3.6 Synthesis of Eu(tta)$_3$DPPZ-COOEt

DPPZ-COOEt (0.0248 g, 0.070 mmol in 5 mL chloroform) was added to a solution of $Eu(tta)_3(H_2O)_2$ (0.0615 g, 0.072 mmol in 5 mL of acetone) and allowed to stir for 30 min at

60°C. Subsequent stirring was done at room temperature for 12 h. The solution was filtered and allowed to evaporate at room temperature yielding the pure product. UV/vis ($CHCl_3$): λ_{max} = 275 nm, 346 nm, 363 nm, 383 nm. Fluorescence ($CHCl_3$, λ_{ex} = 347 nm): λ_{em} = 614 nm, 592 nm, 580 nm, 652 nm. Fluorescence quantum yield (λ_{ex}= 347 nm, reference: cresyl violet in MeOH with Φ = 0.54): 1.04 ± 0.05%.

2.3.7 Synthesis of $Eu(tta)_3$DPPZ-Si Silica Nanoparticles

$Eu(tta)_3$DPPZ-Si (20 mg, 0.0336 mmol) was added to 50 mL of EtOH and allowed to stir at 30°C for 30 min. TEOS (3 mL, 0.0133mmol), NH_4OH (1 mL, 28%), and nanopure H_2O (2 mL) was added to the mixture, heated to 55°C and allowed to stir for 18 h. The solution was centrifuged at 4000 rpm for 20 min, the supernatant fluid was decanted, and the remaining solid particles were allowed to dry at room temperature.

CHAPTER 3: RESULTS AND DISCUSSION

One goal of this project was to develop phenazine based ligands that can absorb light and transfer the energy to the complexed lanthanide (III) ion. In pursuing this goal a number of phenazine ligands were synthesized which contained both electron-donating and electron-withdrawing groups. The hypothesis was that the addition of these groups would perturb the electronic properties of the phenazine ligands and affect their ability to transfer energy to the Eu(III). The goal was to rationally develop a ligand that would be able to optimize the quantum yield of the Eu(III) complex. As of yet, no clear trend suggests itself in regard to the effect of electron donating and withdrawing groups on the quantum yields of the Eu(III) complexes studied.

3.1 Dipyrido[3,2-a:2',3'-c]phenazine Ligand and Eu^{3+} Complex.

3.1.1 Fourier Transform Infrared Spectroscopy Studies

The IR spectrum for dipyrido[3,2-a:2',3'-c]phenazine (DPPZ) shows absorption band at around 3080 cm^{-1} belongs to the aromatic C-H stretch of DPPZ (Figure 8). The absence of absorption bands below the 3000 cm^{-1} is indicative that all the C-H stretches are aromatic in nature with no methyl or methylene groups present. Weak aromatic overtones are apparent in the 2000 cm^{-1} region. The absorption bands from 1400- 1600 cm^{-1} are indicative of C=C ring stretches. The in plane C-H stretches at 1028 and 1074 cm^{-1}, as well as the out of plane C-H stretch at 735 cm^{-1} are a good indication of a successful synthesis of an un-functionalized DPPZ ligand.

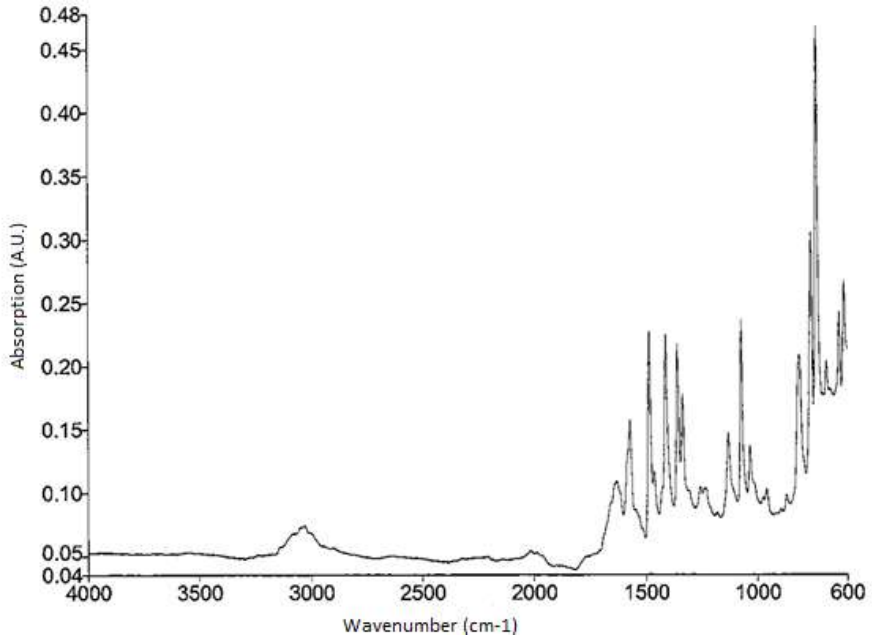

Figure 8. IR spectrum for DPPZ.

The formation of the complex $Eu(tta)_3DPPZ$ via the displacement of water (from $Eu(tta)_3(H_2O)_2$, Figure 9) resulted in changes/shifts in the observed vibrational frequencies of DPPZ. The bands observed between 1400- 1600 cm^{-1} due to the absorption of C=C and C=N ring stretches in DPPZ moved to lower wavenumbers and became more prominent at 1298, 1412, 1538, 1700 cm^{-1} respectively. The absorption band at 2922 cm^{-1} can be attributed to the absorption of C-H stretches (methylene) from tta. While the absorption bands at 1602 and 1132 cm^{-1} belongs to the diketonate carbonyl stretches (C=O) and trifluorene (CF_3) groups from tta respectively. The absorption bands at 736 and 714 cm^{-1} are indicative of the C-H out of plane bending modes for DPPZ.

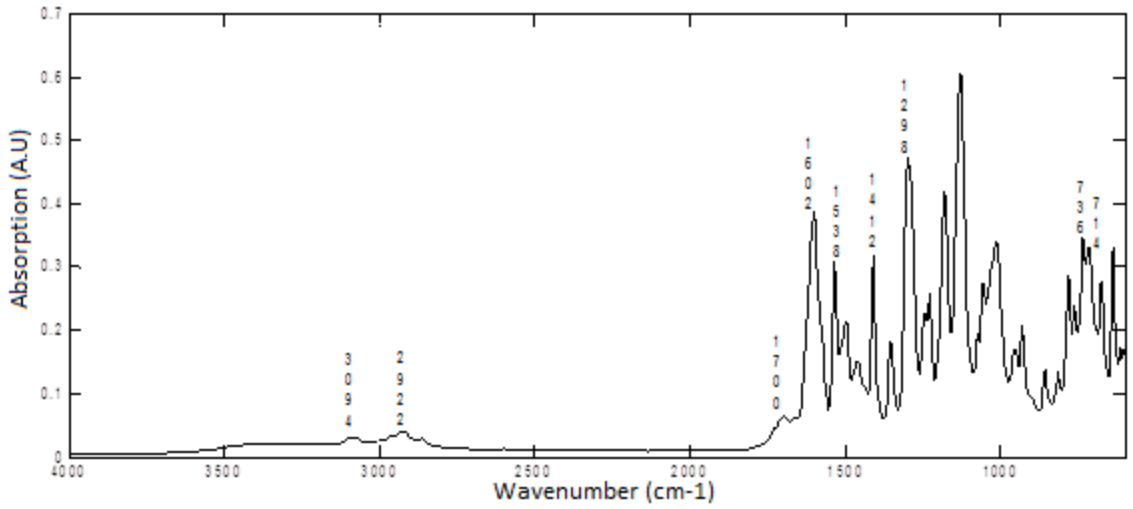

Figure 9. IR spectrum of $Eu(tta)_3DPPZ$.

3.1.2 Ultraviolet-Visible Absorption Spectroscopy Studies

The UV-visible spectra for the ligand (DPPZ) and the complex ($Eu(tta)_3DPPZ$) as well as the starting materials are presented in Figure 10 below. The ligand shows strong absorption spectra with a transition located at 268 nm, with weaker absorption bands occurring at 359 nm and 378 nm regions. The π→π* transition causing the absorption band at 268 nm belongs to the phenanthroline portion of the ligand, while the π→π* transition responsible for the absorption bands at 359 nm and 378 nm are phenazine based. Upon complexation with $Eu(tta)_3(H_2O)_2$ (displacing water), an absorption band characteristic of tta appears at 341 nm. The phenanthroline portion of the ligand responsible for the π→π* transition causing the absorption band at 268 nm shifted to 272 nm. While, the phenazine portion of the ligand responsible for the π→π* transition causing the absorption band at 359 nm and 378 nm experiences a shift to 356 nm and 375 nm respectively, upon complexation.[13]

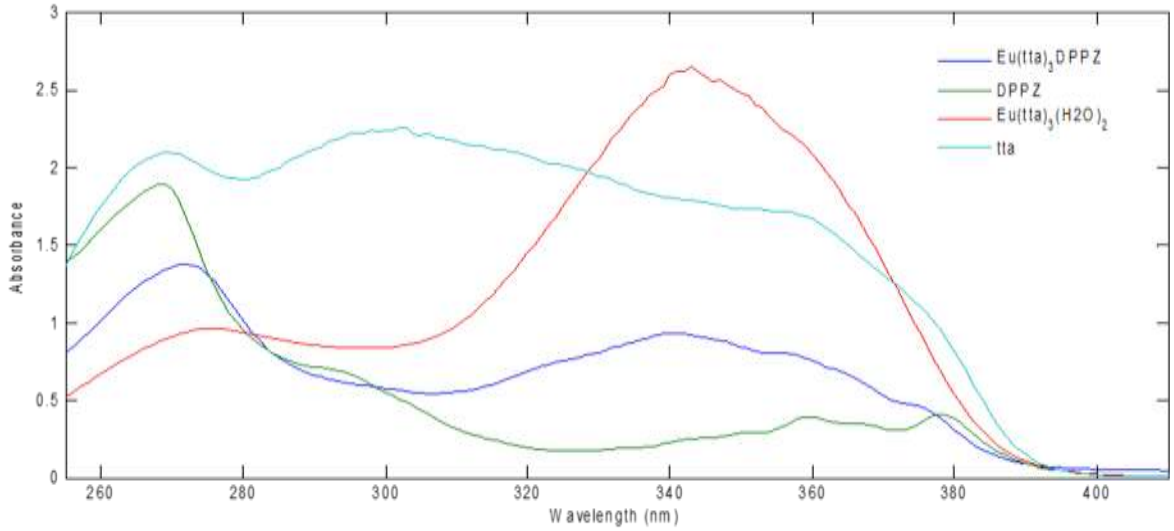

Figure 10. UV-Vis spectra for the ligand (DPPZ), its complex and precursors.

3.1.3 Fluorescence Spectroscopy Studies

The free DPPZ ligand (Figure 11) displayed a fluorescence maximum at around 432 nm (λ_{ex}= 386 nm) while emitting over a range from ~ 400-580 nm.

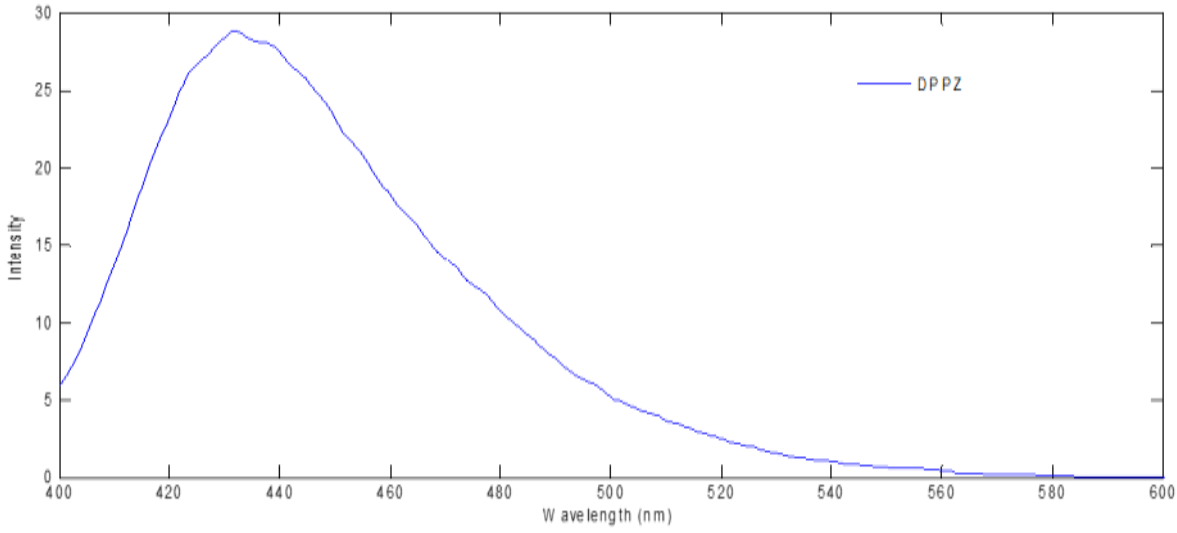

Figure 11. Fluorescence spectrum for DPPZ.

Fluorescence spectra for the $Eu(tta)_3DPPZ$ complex (Figure 12) were measured with 342 nm as the excitation wavelength shows the presence of two emissive states. The narrow peaks

observed in the spectra are the transitions between the $^5D_0$ excited state of Eu^{3+} and the different J levels of the ground term ^7F (^7F_J=0-3).

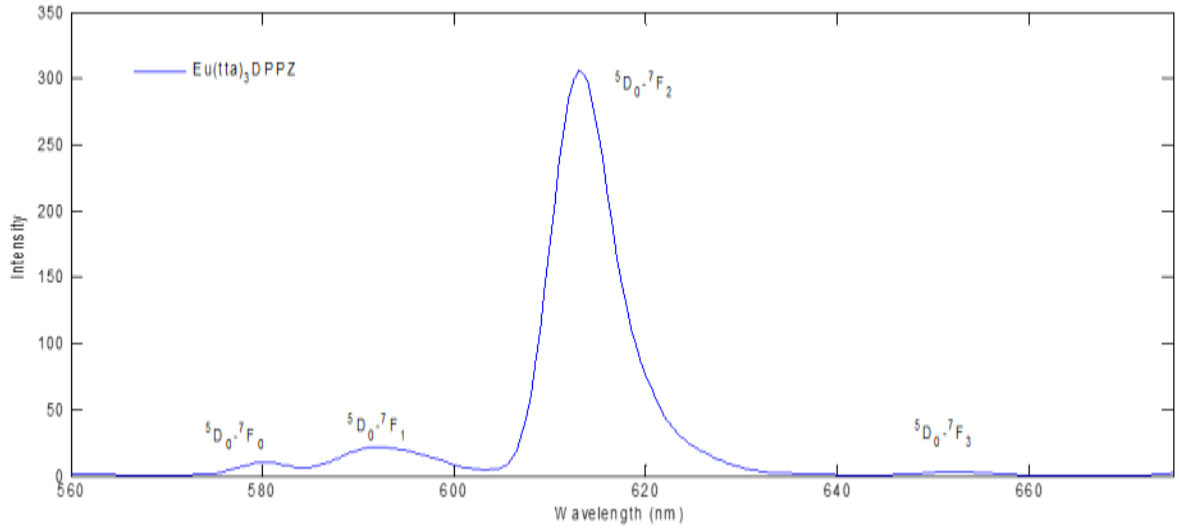

Figure 12. Emissive state transitions for $Eu(tta)_3DPPZ$.

The $^5D_0$-$^7F_2$ transition at λ=613 nm exhibits the strongest emission due to its induced electric dipole transition from its highly polarizable environment around the Eu^{3+} ion. This is the emission is responsible for the bright red luminescence imparted by Eu^{3+} complexes. The intensity of the $^5D_0$-$^7F_1$ transition at λ=592 nm is significantly weaker than that of the $^5D_0$-$^7F_2$ transition due to its independence of the coordination environment as well as primarily being a magnetically induced transition. The $^5D_0$-$^7F_0$ (λ=580 and $^5D_0$-$^7F_3$ (λ=652) are even weaker than the $^5D_0$-$^7F_1$ transition due to their inability to induce a magnetic or electric dipole transition.

The broad emission ranging from 375 nm to 525 nm originates from the energy absorbed by the DPPZ ligand in the complex as observed in Figure 11. When in comparison to the complex fluorescence spectra, the DPPZ ligand was able to transfer energy more efficiently (in comparison to the other functionalized DPPZ ligands) to the Eu(III) ion (Figure 13). No transitions starting from the $^5D_1$ state were observed for this complex.

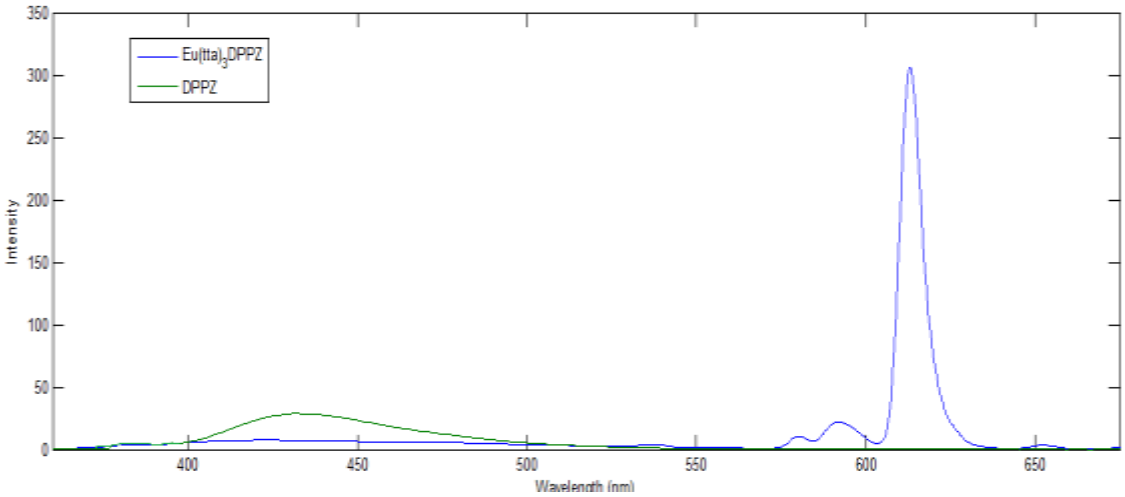

Figure 13. Fluorescence spectra for DPPZ and $Eu(tta)_3DPPZ$.

3.2 Dipyrido[3,2-a:2',3'-c]phenazine-11-methyl Ligand and Eu^{3+} Complex

3.2.1 Fourier Transform Infrared Spectroscopy Studies

The IR spectrum for dipyrido[3,2-a:2',3'-c]phenazine-11-methyl (DPPZ-CH_3, Figure 14) shows an absorption band at around 3050 cm^{-1} that belongs to the aromatic C-H stretch of DPPZ, while the absorption bands in the 2918 cm^{-1} region belong to the saturated methyl C-H stretches. Weak aromatic overtones are apparent in the 1700-2000 cm^{-1} region. The absorption bands from 1400- 1600 cm^{-1} are indicative of C=C ring stretches. The in plane C-H stretches at 1031 and 1071 cm^{-1}, as well as the out of plane C-H stretch at 739 cm^{-1} are indicative of a successful grafting of the methyl group to DPPZ ligand.

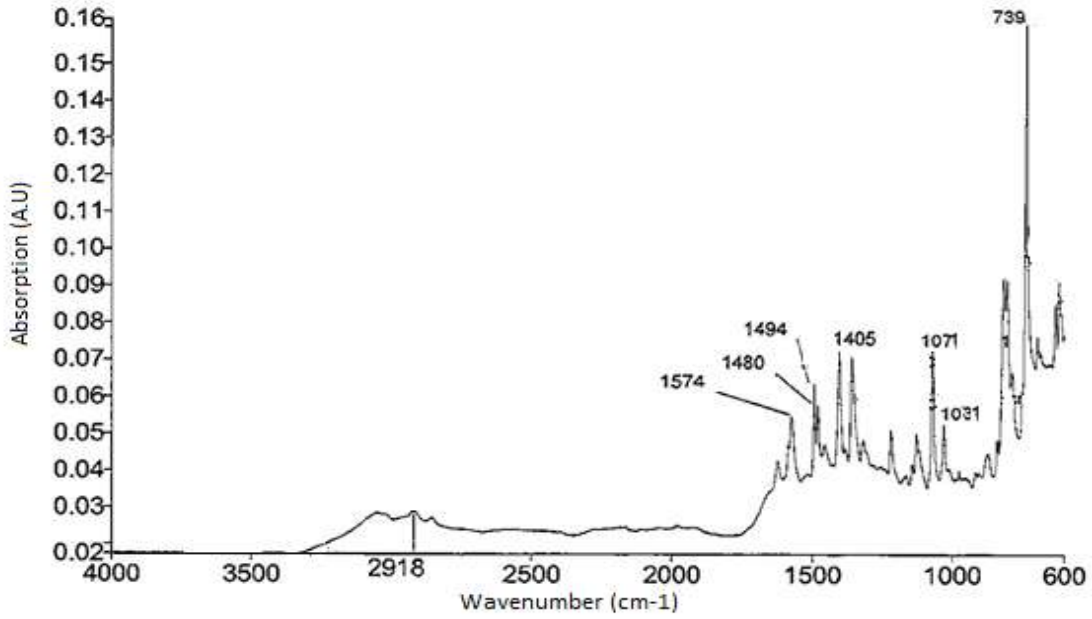

Figure 14. IR spectrum for DPPZ-CH_3.

The formation of the complex Eu(tta)$_3$DPPZ-CH_3 via the displacement of water (from Eu(tta)$_3$(H_2O)$_2$) was not obtained.

3.2.2 Ultraviolet-Visible Absorption Spectroscopy Studies

The UV-visible spectra for the ligand (DPPZ-CH_3) and the complex (Eu(tta)$_3$DPPZ-CH_3) as well as the starting materials are presented in Figure 15 below. The ligand shows strong absorption spectra with a transition located at 273 nm, with weaker absorption bands occurring at 367 nm and 387 nm. The $\pi \rightarrow \pi^*$ transition causing the absorption band 273 nm belongs to the phenanthroline portion of the ligand, while the $\pi \rightarrow \pi^*$ transition responsible for the absorption bands at 367 nm and 387 nm regions are phenazine based. Upon complexation with Eu(tta)$_3$(H_2O)$_2$ (displacing water), an absorption band characteristic of tta appears at 347 nm. The phenanthroline portion of the ligand bound to the metal center responsible for the $\pi \rightarrow \pi^*$ transition is shifted to 272 nm. While, the phenazine portion of the ligand responsible for the $\pi \rightarrow \pi^*$ transition causing the absorption band at 367 and 387 nm shifts to 366 and 386 nm respectively upon complexation.[13]

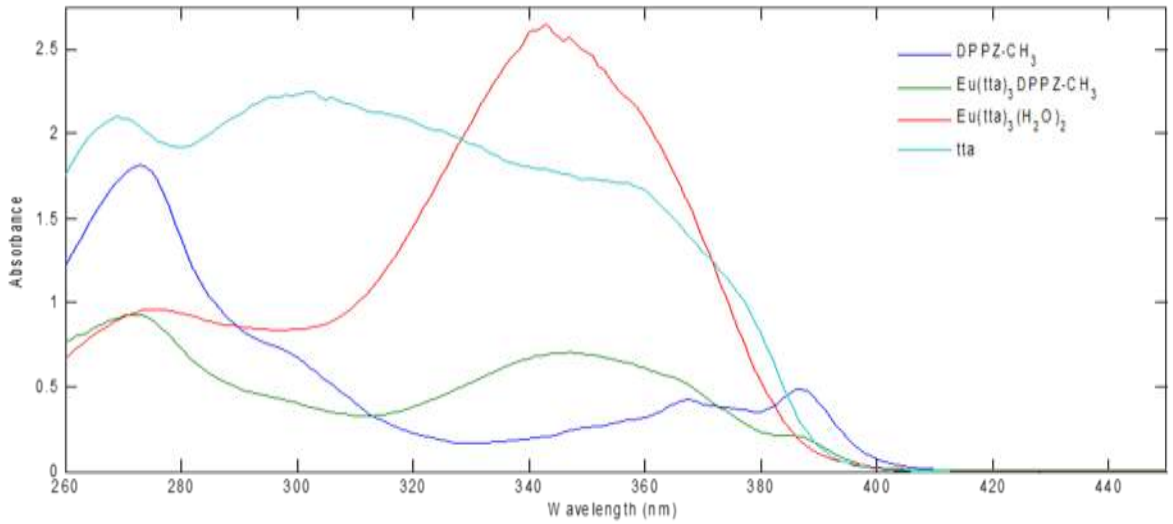

Figure 15. UV-Vis spectra for ligand (DPPZ-CH_3), its complex and precursors.

3.2.3 Fluorescence Spectroscopy Studies

The free DPPZ-CH_3 ligand (Figure 16) displayed a fluorescence maximum at around 413 nm (λ_{ex}= 330 nm) while emitting over a range from ~ 375-650 nm.

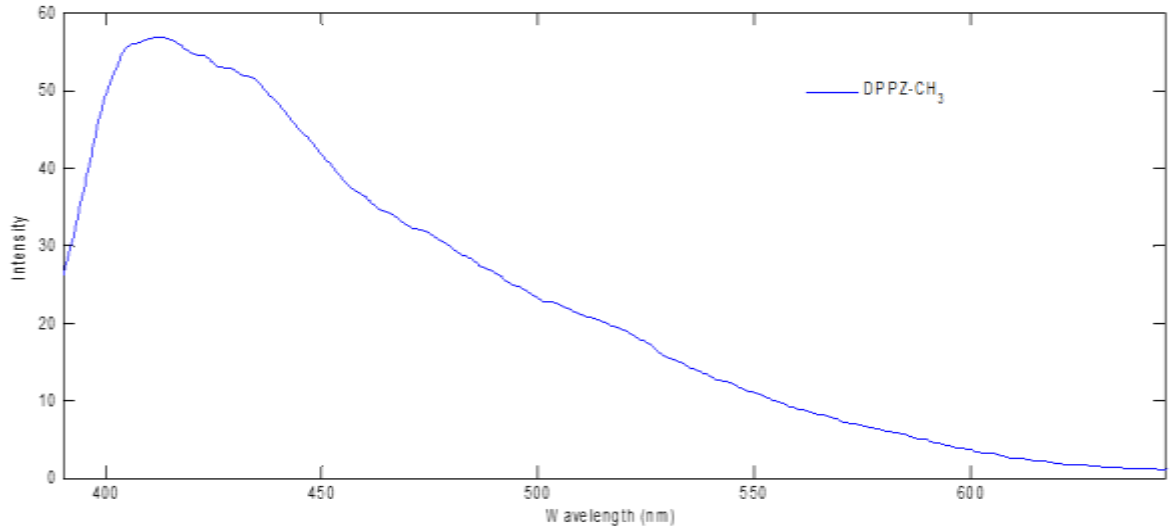

Figure 16. Fluorescence spectrum for DPPZ-CH_3.

Fluorescence spectra for the Eu(tta)$_3$DPPZ-CH_3 complex (Figure 17) were measured with 349 nm as the excitation wavelength shows the presence of two emissive states. The narrow peaks

observed in the spectra are the transitions between the $^5D_0$ excited state of Eu^{3+} and the different J levels of the ground term ^7F (^7F_J=0-3).

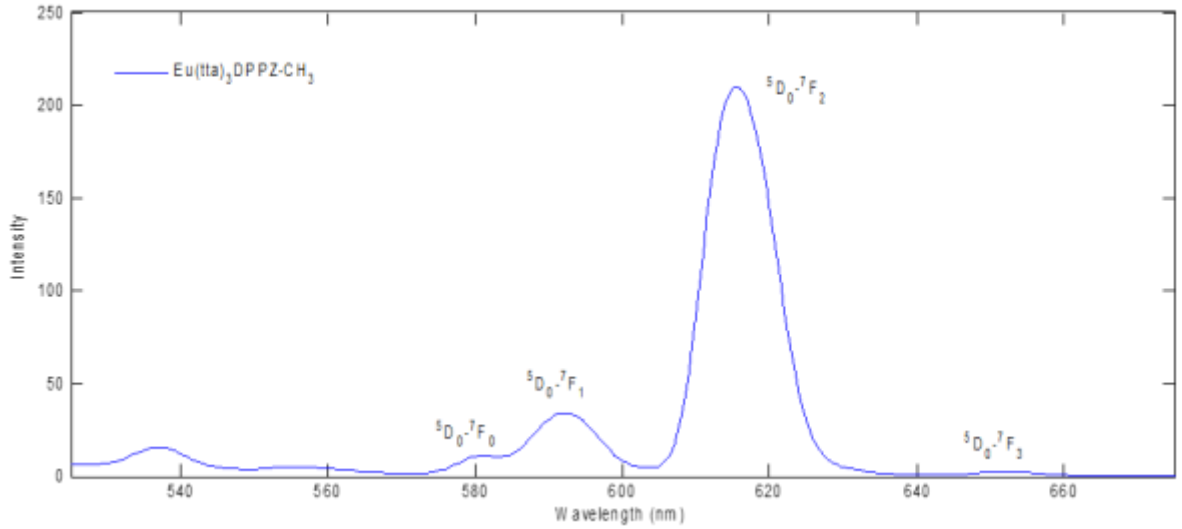

Figure 17. Emissive state transitions for $Eu(tta)_3DPPZ\text{-}CH_3$.

The $^5D_0$-$^7F_2$ transition at λ=616 nm exhibits the strongest emission due to its induced electric dipole transition from its highly polarizable environment around the Eu^{3+} ion. This is emission is responsible for the bright red luminescence imparted by Eu^{3+} complexes. The intensity of the $^5D_0$-$^7F_1$ transition at λ=592 nm is significantly weaker than that of the $^5D_0$-$^7F_2$ transition due to its independence of the coordination environment as well as primarily being a magnetically induced transition. The $^5D_0$-$^7F_0$ (λ=581) and $^5D_0$-$^7F_3$ (λ=652) are even weaker than the $^5D_0$-$^7F_1$ transition due to their inability to induce a magnetic or electric dipole transition. Transitions starting from the $^5D_1$ state were also observed for this complex at 537 nm ($^5D_1$-$^7F_1$) and 555 nm ($^5D_1$-$^7F_2$) due to energy transfer from the singlet excited state of the ligand to the Eu^{3+} excited state associate with the $^5D_1$ energy level.[27]

The broad emission ranging from 350 nm to 525 nm originates from the energy absorbed by the $DPPZ\text{-}CH_3$ ligand in the complex as observed in Figure 16. When in comparison to the

complex fluorescence spectra, the DPPZ-CH_3 ligand was able to transfer minimal energy to the Eu(III) ion (Figure 18) which is indicative of a lower triplet energy state than that of europium.

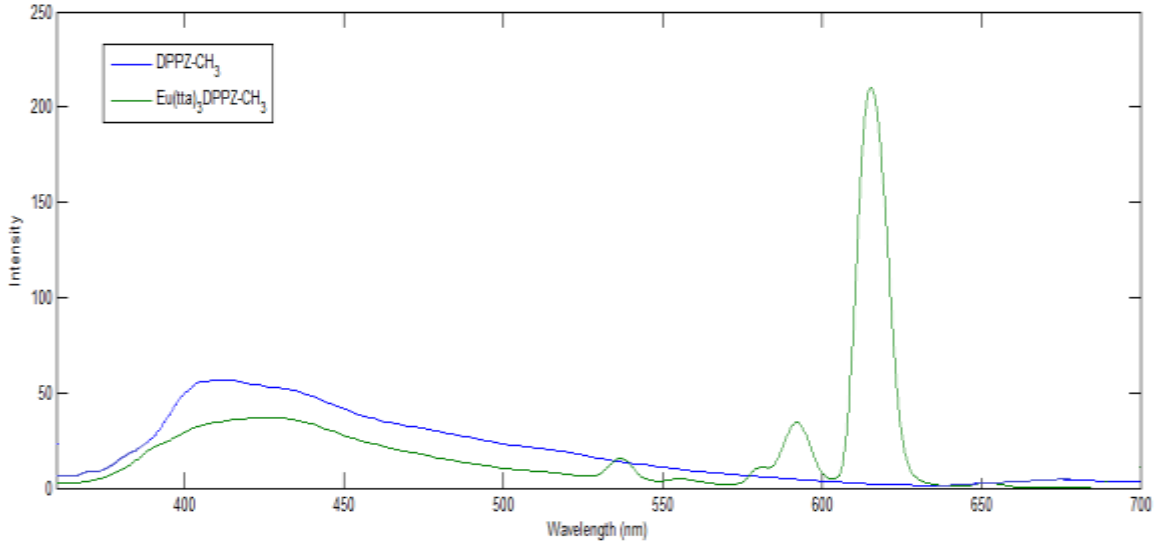

Figure 18. Fluorescence spectra for DPPZ-CH_3 and $Eu(tta)_3$DPPZ-CH_3.

3.3 Dipyrido[3,2-a:2',3'-c]phenazine-11-carboxylic acid Ligand and Eu^{3+} Complex

3.3.1 Fourier Transform Infrared Spectroscopy Studies

The IR spectrum for dipyrido[3,2-a:2',3'-c]phenazine-11-carboxylic acid (Figure 19) shows a broad absorption band in the range of 2500-3250 cm^{-1} that can be attributed to an O-H stretch. The absorption band at 1713 cm^{-1} belongs to the asymmetric carbonyl (C=O) stretch of the carboxylic acid. This, along with the O-H stretch, is indicative that the carboxylic acid group was successfully attached at site 11 of the DPPZ ligand.

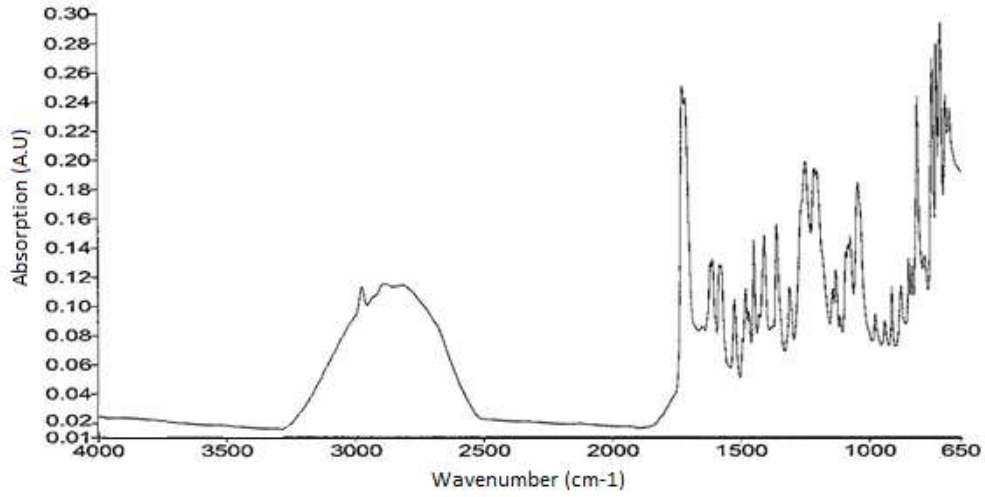

Figure 19. IR spectrum for DPPZ-COOH.

The infrared spectrum of the formation of the complex $Eu(tta)_3$DPPZ-COOH via the displacement of water (from $Eu(tta)_3(H_2O)_2$) was not obtained.

3.3.2 Ultraviolet-Visible Absorption Spectroscopy Studies

The UV-visible spectra for the ligand (DPPZ-COOH) and the complex ($Eu(tta)_3$DPPZ-COOH) as well as the starting materials are presented in Figure 20 below. The ligand shows strong absorption spectra with a transition located at 275 nm, with weaker absorption bands occurring at 369 nm and 388 nm. The $\pi \rightarrow \pi^*$ transition causing the absorption band at 275 nm region belongs to the phenanthroline portion of the ligand, while the $\pi \rightarrow \pi^*$ transition responsible for the absorption bands in the 369 nm and 388 nm regions are phenazine based. Upon complexation with $Eu(tta)_3(H_2O)_2$ (displacing water), an absorption band characteristic of tta appears at 346 nm. The phenanthroline portion of the ligand bound to the metal center responsible for the $\pi \rightarrow \pi^*$ transition experiences a shift to 273 nm. While, the phenazine portion of the ligand responsible for the $\pi \rightarrow \pi^*$ transition causing the absorption band at 369 nm and 388 nm appears to have disappeared upon complexation.[13]

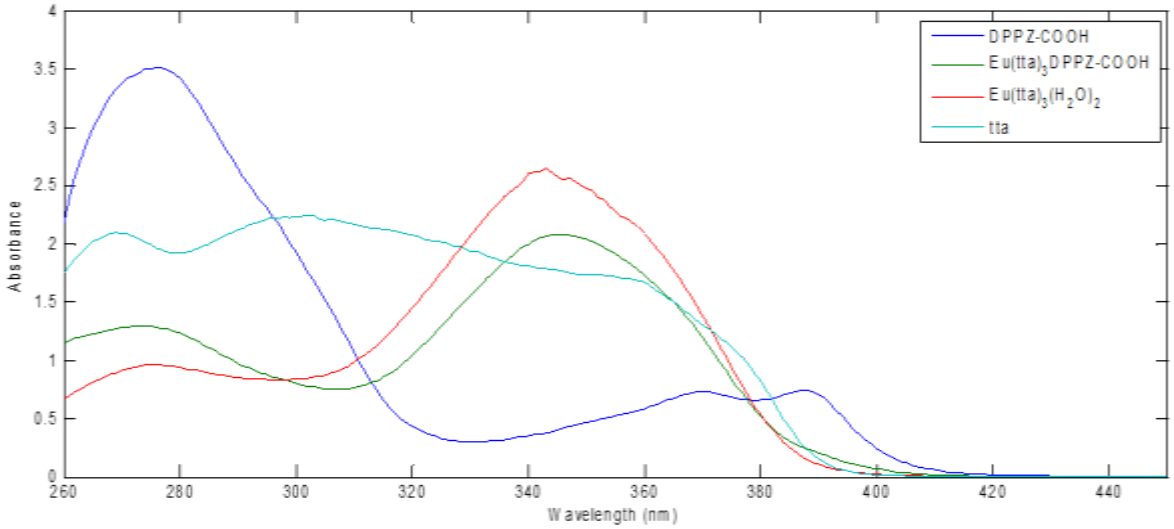

Figure 20. UV-Vis spectra for ligand (DPPZ-COOH), its complex and precursors.

3.3.3 Fluorescence Spectroscopy Studies

The free DPPZ-COOH ligand (Figure 21) displayed a fluorescence maximum at 521 nm (λ_{ex}= 320 nm) while emitting over a range from ~ 380-625 nm. The broad emission ranging from 375 nm to 500 nm from the energy absorbed by the DPPZ-COOH ligand in the complex as observed in Figure 21. It was determined that the large peak at 521 nm for the ligand was the result of an excimer, which explains why DPPZ-COOH has a different emission spectrum in comparison to the other functionalized DPPZ ligands.

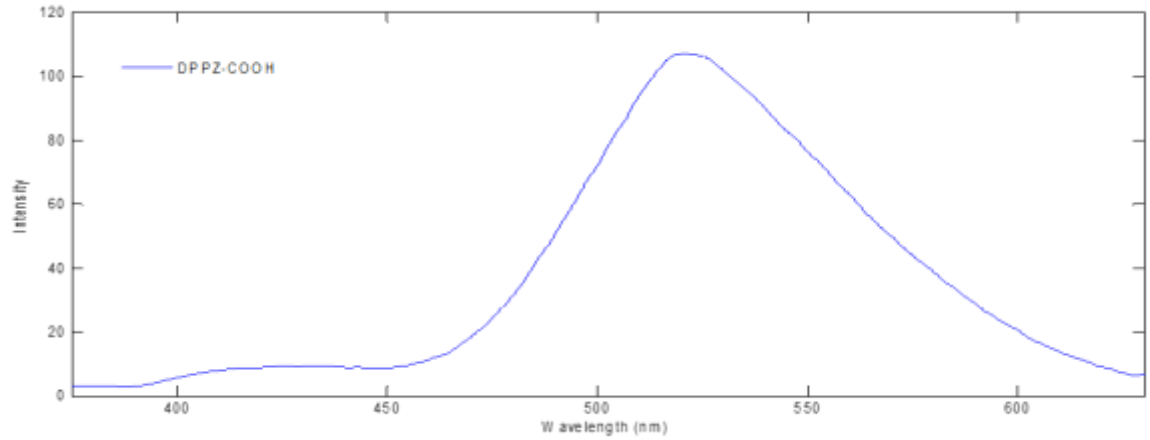

Figure 21. Fluorescence spectrum for DPPZ-COOH.

Fluorescence spectra for the $Eu(tta)_3DPPZ\text{-}COOH$ complex (Figure 22) were measured with 349 nm as the excitation wavelength shows the presence of two emissive states. The narrow peaks observed in the spectra are the transitions between the $^5D_0$ excited state of Eu^{3+} and the different J levels of the ground term ^7F (^7F_J=0-3).

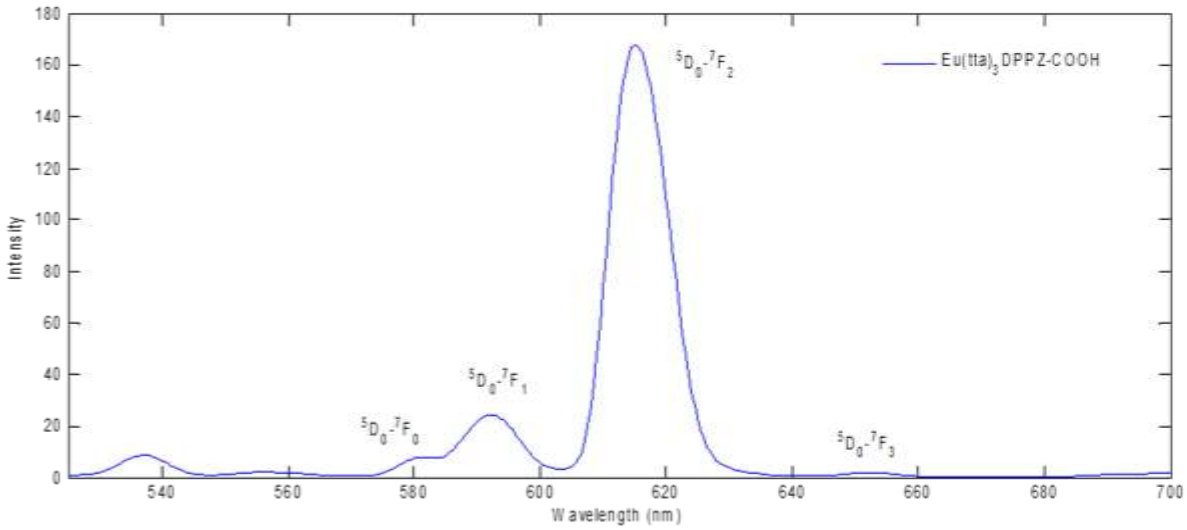

Figure 22. Emissive state transitions for $Eu(tta)_3DPPZ\text{-}COOH$.

The $^5D_0$-$^7F_2$ transition at λ=615 nm exhibits the strongest emission due to its induced electric dipole transition from its highly polarizable environment around the Eu^{3+} ion. This is emission is responsible for the bright red luminescence imparted by Eu^{3+} complexes. The intensity of the $^5D_0$-$^7F_1$ transition at λ=592 nm is significantly weaker than that of the $^5D_0$-$^7F_2$ transition due to its independence of the coordination environment as well as primarily being a magnetically induced transition. The $^5D_0$-$^7F_0$ (λ=581 and $^5D_0$-$^7F_3$ (λ=652) are even weaker than the $^5D_0$-$^7F_1$ transition due to their inability to induce a magnetic or electric dipole transition. Transitions starting from the $^5D_1$ state were also observed for this complex at 537 nm ($^5D_1$-$^7F_1$) and 556 nm ($^5D_1$-$^7F_2$) due to energy transfer from the singlet excited state of the ligand to the Eu^{3+} excited state associated with the $^5D_1$ energy level.[27]

When in comparison to the complex fluorescence spectra, the DPPZ-COOH ligand weak emission was able to transfer minimal energy to the Eu(III) ion (Figure 23) which is indicative of a lower triplet energy state than that of europium.

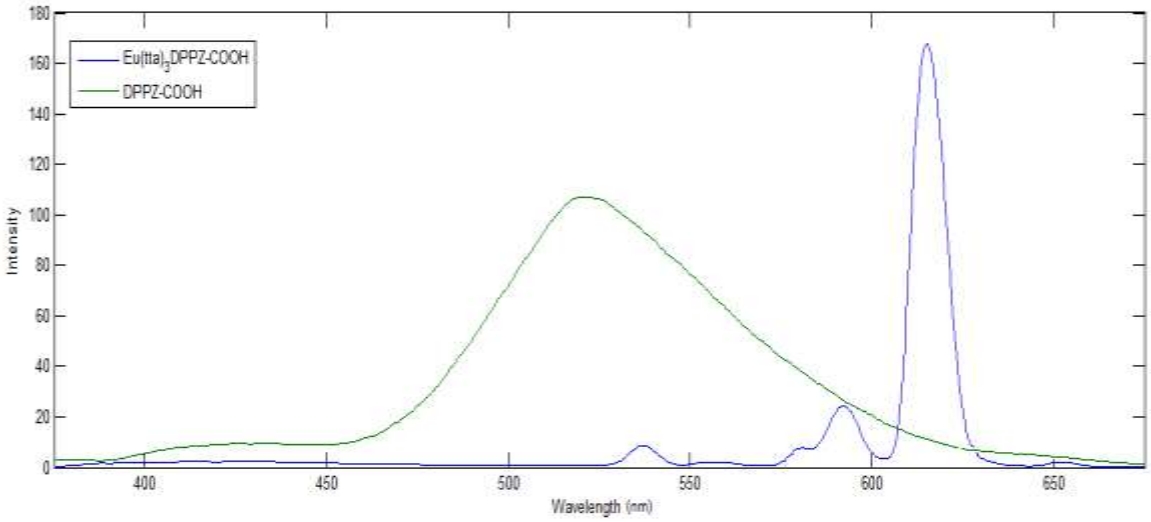

Figure 23. Fluorescence spectra for DPPZ-COOH and $Eu(tta)_3$DPPZ-COOH.

3.4 Dipyrido[3,2-a:2',3'-c]phenazine-11-ethyl ester Ligand and Eu^{3+} Complex

3.4.1 Fourier Transform Infrared Spectroscopy Studies

The IR spectrum for dipyrido[3,2-a:2',3'-c]phenazine-11-ethyl ester (DPPZ-COOEt, Figure 24). The absorption band at 1713 cm^{-1} that was apparent in DPPZ-COOH belonging to the asymmetric carbonyl stretch of the carboxylic acid has shifted to 1711 cm^{-1} for the asymmetric carbonyl stretch of the ethyl ester. The absorption band corresponding to a C(=O)-O stretch at 1204 cm-1, along with the asymmetric carbonyl stretch is indicative of a successful grafting of the ethyl ester functional group to the DPPZ ligand. Aromatic C-H stretches from are responsible for the absorption band at 3016 cm^{-1}. While the absorption bands in the 2943 region are responsible for the C-H stretches of the methyl and methylene portions of the ethyl group attached to the carbonyl. The C-C stretch at 1406 cm^{-1} along with the absorption bands

corresponding to the C-H stretches of the ethyl group is further evidence of a successful substitution of the ethyl ester to the DPPZ ligand.

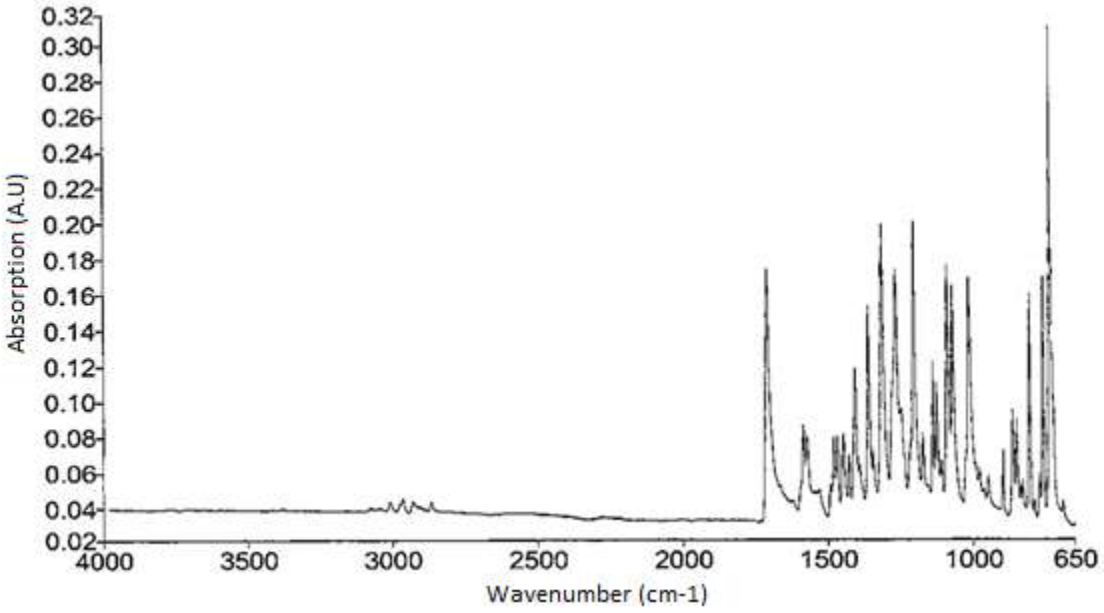

Figure 24. IR spectrum for DPPZ-COOEt.

The formation of the complex $Eu(tta)_3$DPPZ-COOEt (Figure 25) via the displacement of water (from $Eu(tta)_3(H_2O)_2$) resulted in changes/shifts in the observed vibrational frequencies of DPPZ-COOEt. The bands observed at 1711 and 1204 cm^{-1} due to the absorption of C=O and C(=O)-O stretches in DPPZ-COOEt were shifted up field to 1719 and downfield to 1184 cm^{-1} respectively. The aromatic C-H stretches from DPPZ-COOEt and tta are responsible for the absorption band at 3091 cm^{-1}. The C-H stretches at 2943 cm^{-1} (methyl, DPPZ-COOEt) were shifted to 2957 cm^{-1}, and the stretches around 2930 cm^{-1} (methylene, DPPZ-COOEt) are responsible for the increase in absorption for this region. The absorption bands at 1597 and 1133 cm^{-1} belong to the diketonate carbonyl stretches (C=O) and the trifluorene (CF_3) groups from tta respectively. These absorption bands are indicative of a successful coordination of DPPZ-COOEt and tta to the complex.

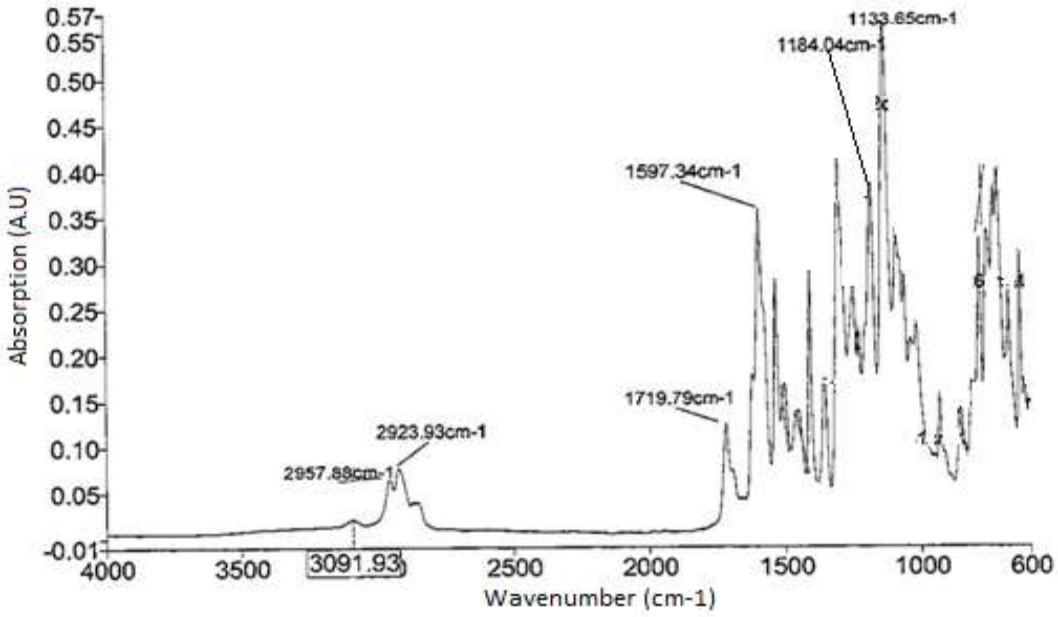

Figure 25. IR spectrum for $Eu(tta)_3DPPZ\text{-}COOEt$.

3.4.2 Ultraviolet-Visible Absorption Spectroscopy Studies

The UV-visible spectra for the ligand (DPPZ-COOEt) and the complex ($Eu(tta)_3DPPZ$-COOEt) as well as the starting materials are presented in Figure 26 below. The ligand shows strong absorption spectra with a transition located at 277 nm, with weaker absorption bands occurring at 366 nm and 386 nm. The $\pi \rightarrow \pi^*$ transition causing the absorption band at 277 nm region belongs to the phenanthroline portion of the ligand, while the $\pi \rightarrow \pi^*$ transition responsible for the absorption bands at 366 nm and 386 nm are phenazine based. Upon complexation with $Eu(tta)_3(H_2O)_2$ (displacing water), an absorption band characteristic of tta appears at 346 nm region. The phenanthroline portion of the ligand responsible for the $\pi \rightarrow \pi^*$ transition causing the absorption band at 277 nm experiences a shift to 275 nm. While, the phenazine portion of the ligand responsible for the $\pi \rightarrow \pi^*$ transitions causing the absorption bands at 366 and 386 nm experience a shift to 363 and 383 nm upon complexation.[13]

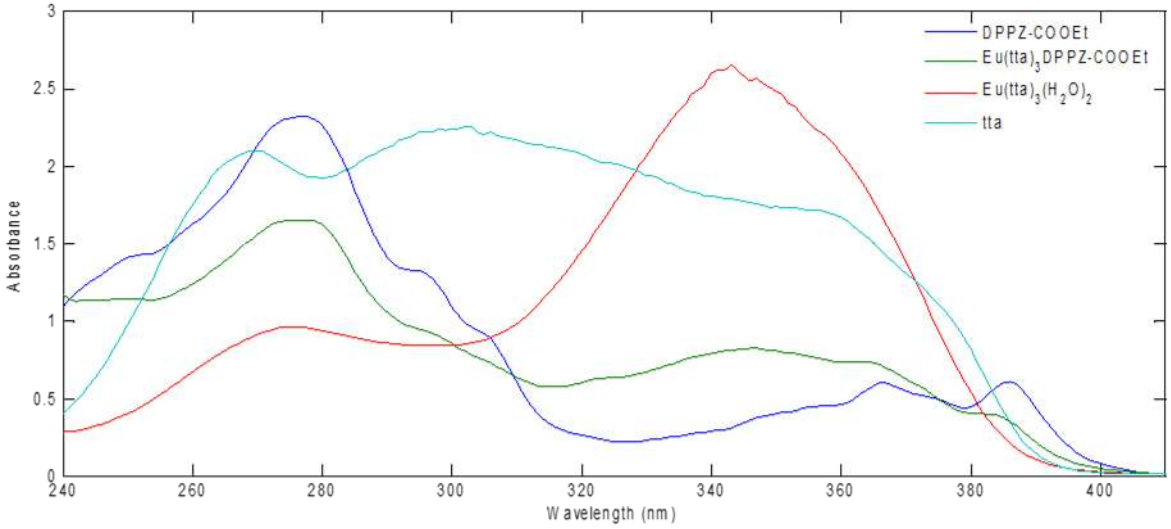

Figure 26. UV-Vis spectra for the ligand (DPPZ-COOEt), its complex and precursors.

3.4.3 Fluorescence Spectroscopy Studies

The free DPPZ-COOEt ligand (Figure 27) displayed a fluorescence maximum at around 435 nm (λ_{ex}= 386 nm) while emitting over a range from ~ 400-570 nm.

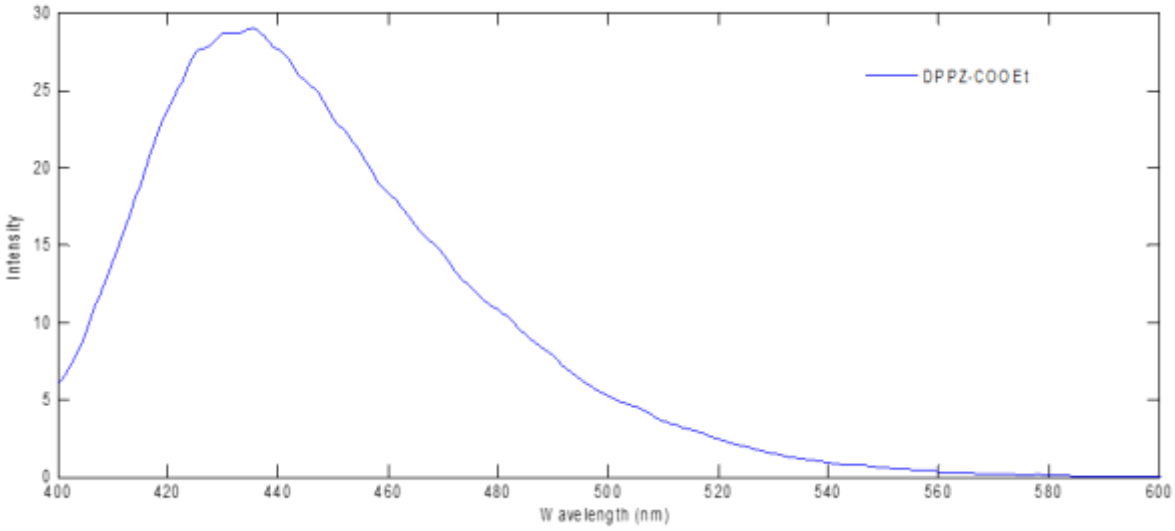

Figure 27. Fluorescence spectrum for DPPZ-COOEt.

Fluorescence spectrum for the $Eu(tta)_3$DPPZ-COOEt complex (Figure 28) were measured with 347 nm as the excitation wavelength shows the presence of two emissive states. The narrow

peaks observed in the spectra are the transitions between the $^5D_0$ excited state of Eu^{3+} and the different J levels of the ground term ^7F (^7F_J=0-3).

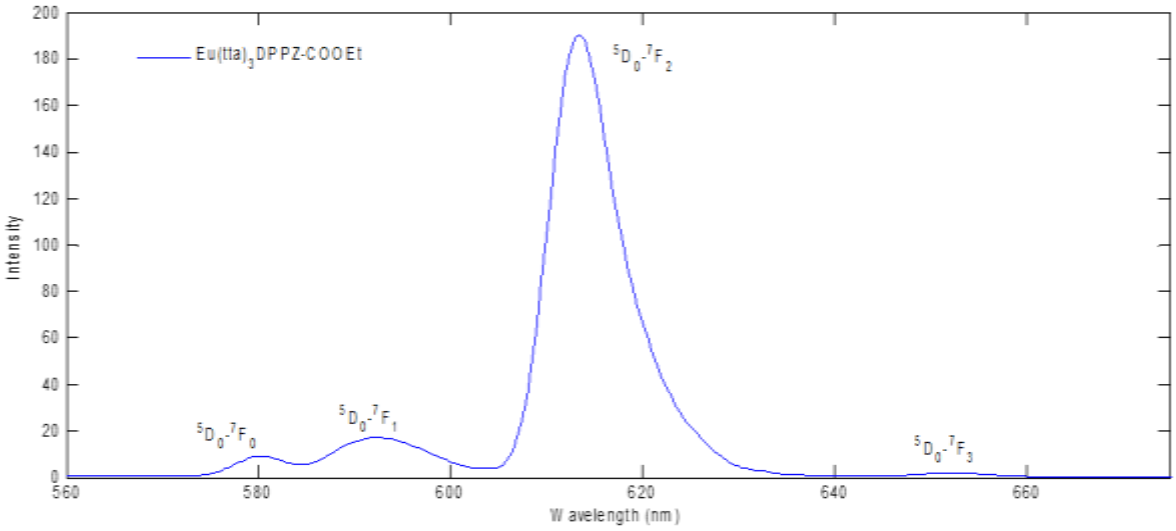

Figure 28. Emissive state transitions for $Eu(tta)_3DPPZ$-COOEt.

The $^5D_0$-$^7F_2$ transition at λ=614 nm exhibits the strongest emission due to its induced electric dipole transition from its highly polarizable environment around the Eu^{3+} ion. This is emission is responsible for the bright red luminescence imparted by Eu^{3+} complexes. The intensity of the $^5D_0$-$^7F_1$ transition at λ=592 nm is significantly weaker than that of the $^5D_0$-$^7F_2$ transition due to its independence of the coordination environment as well as primarily being a magnetically induced transition. The $^5D_0$-$^7F_0$ (λ=580) and $^5D_0$-$^7F_3$ (λ=652) are even weaker than the $^5D_0$-$^7F_1$ transition due to their inability to induce a magnetic or electric dipole transition.

While the broad emission ranging from 400 nm to 570 nm originates from the energy absorbed by the DPPZ-COOEt ligand in the complex as observed in Figure 27. When in comparison to the complex fluorescence spectra, the DPPZ-COOEt ligand was able to transfer more energy to the Eu(III) ion than all of the other complexes except $Eu(tta)_3DPPZ$ (Figure 29). No transitions starting from the $^5D_1$ state were observed for this complex. The significant

decrease in quantum yield in comparison to $Eu(tta)_3DPPZ$ suggests that the triplet state energy level for DPPZ-COOEt is still lower than that of the Eu (III) ion.

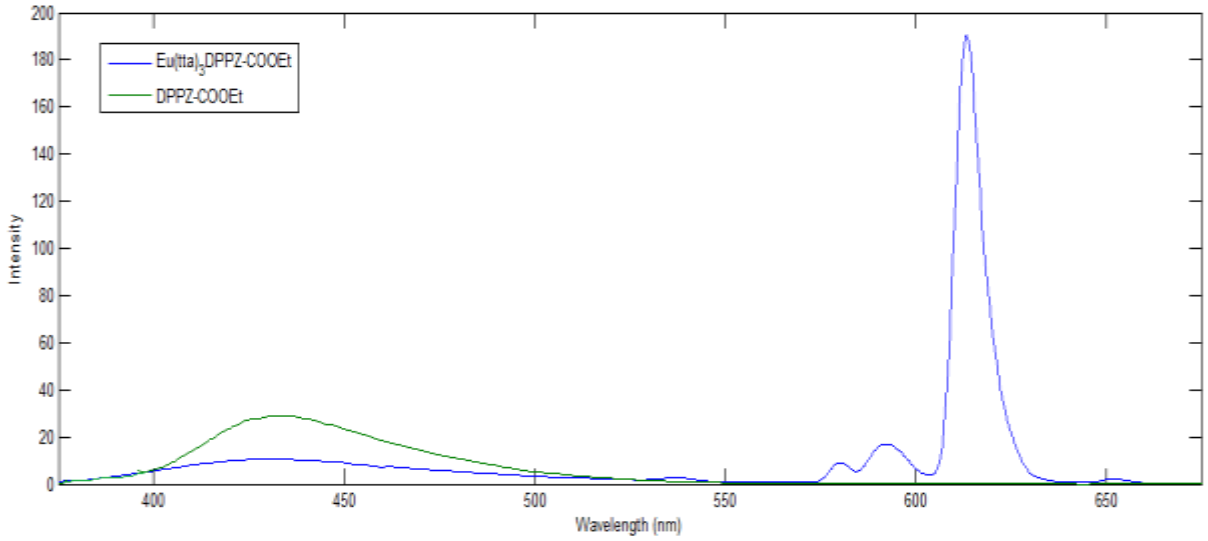

Figure 29. Fluorescence spectra for DPPZ-COOEt and $Eu(tta)_3DPPZ$-COOEt.

3.5 Dipyrido[3,2-a:2',3'-c]phenazine-11-carboxamide,N –[3-triethoxy)propyl]Ligand, Eu^{3+} Complex, and $Eu(tta)_3$DPPZ-Si silica bound nanoparticles.

3.5.1 Fourier Transform Infrared Spectroscopy Studies

The IR spectrum for dipyrido[3,2-a:2',3'-c]phenazine-11-carboxamide,N –[3-triethoxy)propyl] (DPPZ-Si, Figure 30). The absorption band at 1713 cm^{-1} that was apparent in DPPZ-COOH belonging to the asymmetric carbonyl stretch of the carboxylic acid is replaced by bands at 1653 and 1638 cm^{-1} due to the absorption of amide groups. This indicates that APTS was successfully coupled to the DPPZ ligand. The secondary amide stretching at 3278 cm^{-1} and bending at 1547 cm^{-1}, the Si-C stretching at 793 cm^{-1} as well as the Si-O stretching vibration at 1070 cm^{-1}, the alkoxy C-H stretches at 2963 cm^{-1} (methyl) and 2930 cm^{-1} (methylene) also gives the expected vibrational modes indicative of the successful addition of APTS to DPPZ.[14]

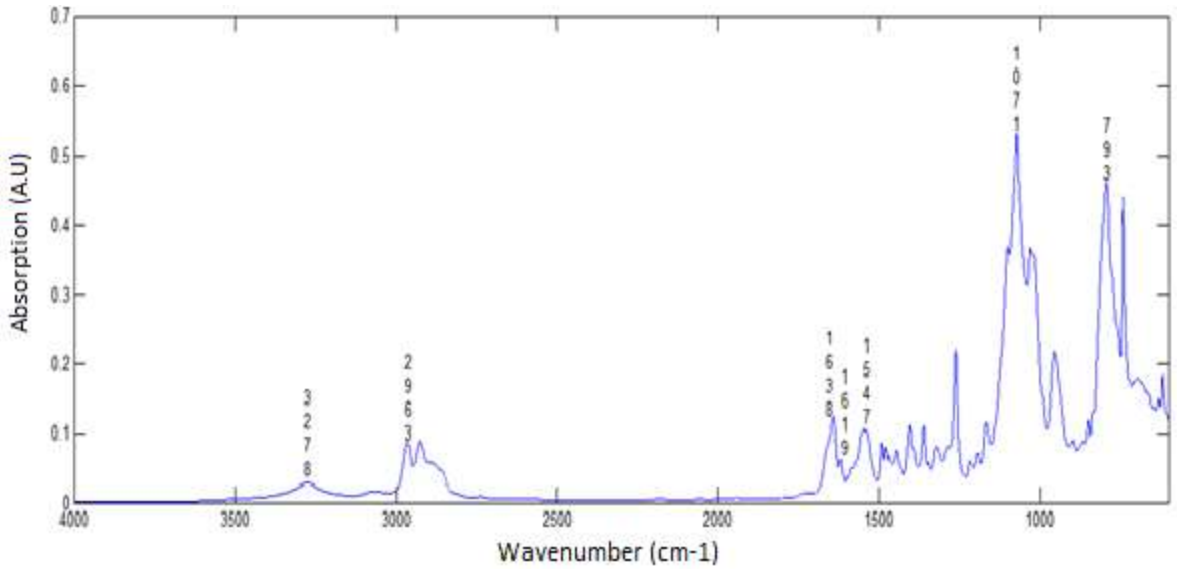

Figure 30. IR spectrum of DPPZ-Si.

The formation of the complex $Eu(tta)_3$DPPZ-Si (Figure 31) via the displacement of water (from $Eu(tta)_3(H_2O)_2$) resulted in changes/shifts in the observed vibrational frequencies of DPPZ-Si. The broad absorption band observed for $Eu(tta)_3(H_2O)_2$ around 3000-3500cm^{-1} belonging to the water molecules bound to the complex are absent, confirming they have been replaced by the bidentate donors of DPPZ-Si. The bands observed at 1653 and 1638 cm^{-1} due to the absorption of amide groups in DPPZ-Si were blue shifted to 1622 and 1602 cm^{-1} respectively. The secondary amide stretching at 3278 cm^{-1} and bending at 1547 cm^{-} observed for the ligand was found to be weakly absorbing at 3212 cm^{-1} and 1538 cm^{-1} respectively. The Si-O stretching vibration at 1070 cm^{-1} dissipated upon coordination to the complex, and became more prominent at 1090 cm^{-1}. The reduction of absorption could be attributed to the less overall concentration of the ligand in the complex, and the shift downfield is indicative of the lack of involvement in the phenazine portion of the ligand in the coordination to the Eu^{3+} ion. The alkoxy C-H stretches at 2963 cm^{-1} (methyl) were shifted to 2954 cm^{-1}, and the stretches around 2930 cm^{-1} (methylene) showed a shift to 2918 cm^{-1} as well as an increase in absorption which could be attributed to the

absorption of C-H stretches (methylene) from tta. The absorption band at 1716 cm^{-1} belongs to the diketonate carbonyl stretches (C=O) from tta. The Si-C absorption band at 798 cm^{-1} indicates that the silane coupling agent maintained its bonds with DPPZ during the coordination process.[14]

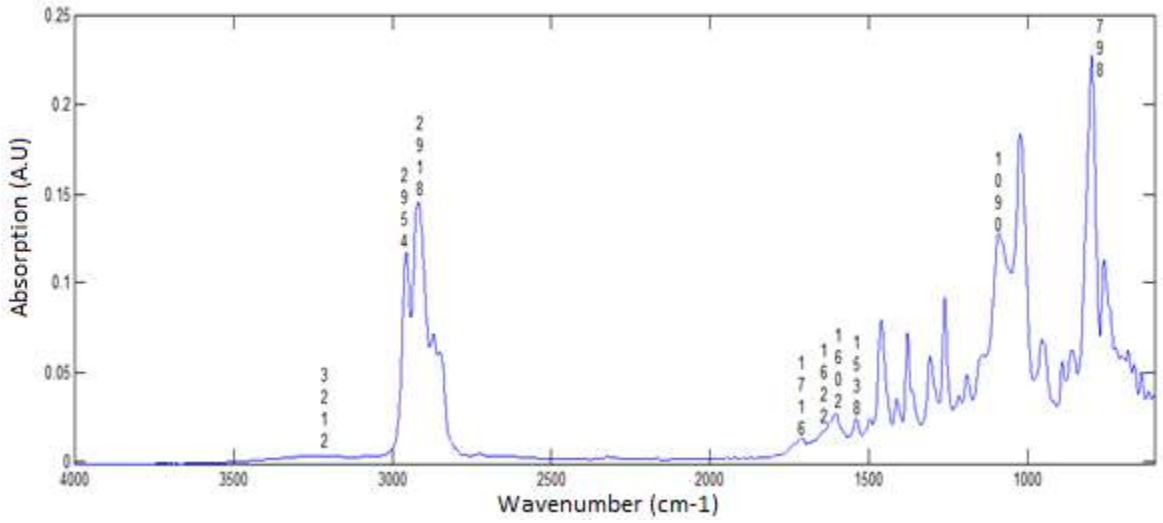

Figure 31. IR spectrum of $Eu(tta)_3$DPPZ-Si.

The addition of TEOS, ethanol, and water to $Eu(tta)_3$DPPZ-Si in the formation of the silica nanoparticle (Figure 32) is responsible for the changes in the IR spectra due to the hydrolysis and condensation of TEOS and DPPZ-Si. The intense broad absorption band around 1110 cm^{-1} is indicative of the formation of siloxane (Si-O-Si) bonds between TEOS and DPPZ-Si, and the Si-C bond at 796 cm-1 is indicative of the silane coupling agent still being bound to the ligand. This is expected since no Si-C bond cleavage is supposed to occur during hydrolysis and subsequent condensation reactions. Due to the absence of intense absorption bands, characteristic of O-H stretching (from Si-OH, EtOH or H_2O) in the range of 3200-3700 cm^{-1}, there is no silanol or water present within the silica matrix. The absorption band at around 950 cm^{-1} is likely due to Si-O-C_2H_5 vibrations.[20] Since no Si-C bond cleavage occurs during hydrolysis/condensation, it is believed that unbound $Eu(tta)_3$DPPZ-Si is encased within the

nanoparticle matrix. Also, with the lack of prominent absorption bands (as discussed for $Eu(tta)_3$DPPZ-Si) apparent, the formation of a thick, multi-layered silica matrix is thought to have occurred. This would explain the lack of absorption observed due to the evanescence field's ability to achieve a penetration depth of only a few microns (0.5-2) into the sample.

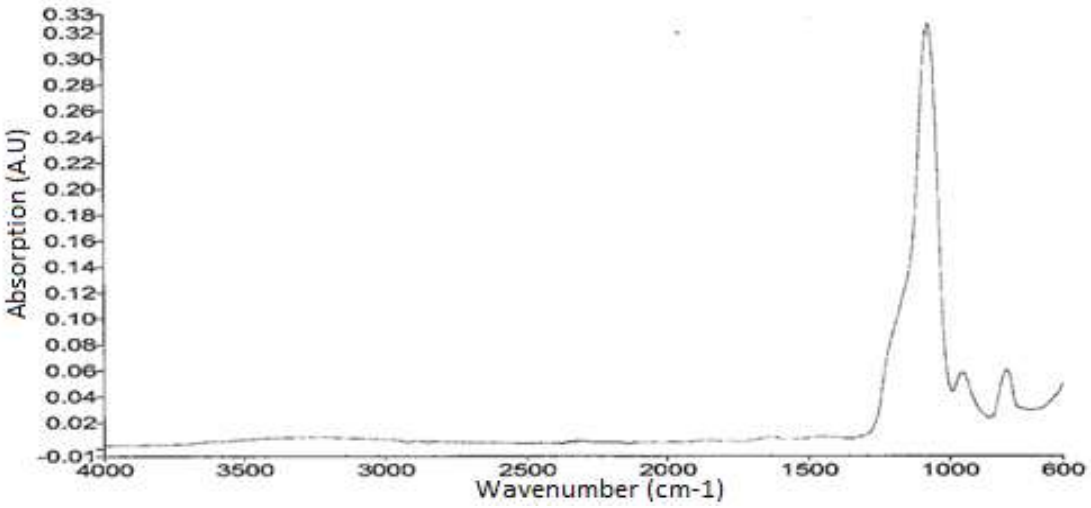

Figure 32. IR spectrum of $Eu(tta)_3$DPPZ-Si silica nanoparticle.

3.5.2 Ultraviolet-Visible Absorption Spectroscopy Studies

The UV-visible spectra for the ligand (DPPZ-Si) and the complex ($Eu(tta)_3$DPPZ-Si) as well as the starting materials are presented in Figure 33 below. The ligand shows strong absorption spectra with a transition located at 269 nm, with weaker absorption bands occurring in the 367 nm and 385 nm. The $\pi \rightarrow \pi^*$ transition causing the absorption band at 269 nm region belongs to the phenanthroline portion of the ligand, while the $\pi \rightarrow \pi^*$ transition responsible for the absorption bands in the 367 nm and 385 nm regions is phenazine based. Upon complexation with $Eu(tta)_3(H_2O)_2$ (displacing water), an absorption band characteristic of the electronic transition of the aromatic rings in the β-diketonate (tta) appears at 346 nm. The phenanthroline portion of the ligand responsible for the $\pi \rightarrow \pi^*$ transition causing the absorption band at 269 nm is shifted to 279 nm, and the phenazine portion of the ligand responsible for the $\pi \rightarrow \pi^*$ transition

causing the absorption band at 367 and 385 nm shifts to 363 and 383 nm respectively upon complexation.[13]

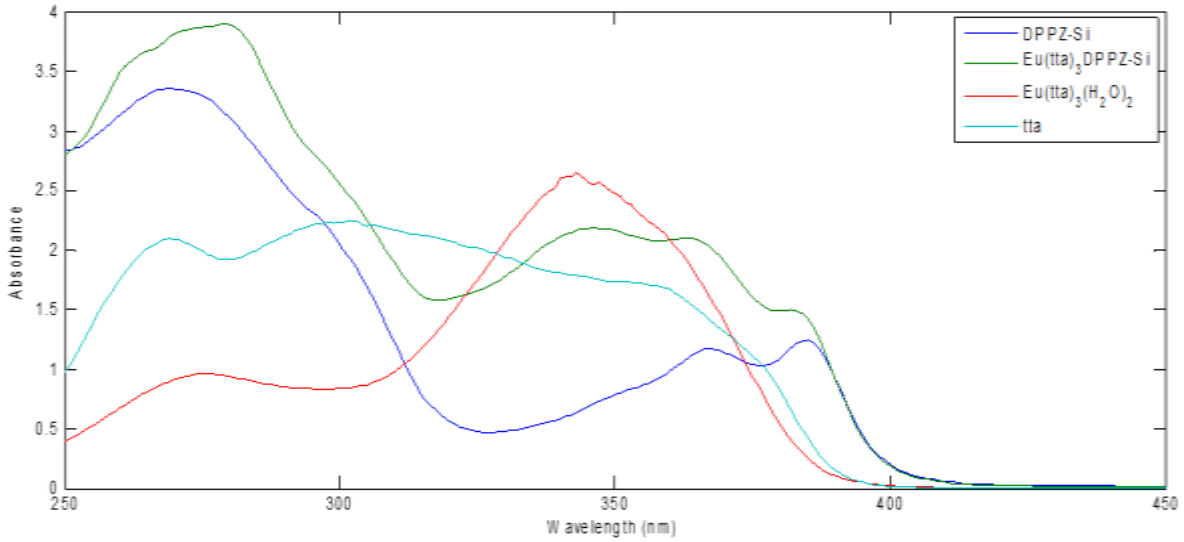

Figure 33. UV-Vis spectra for the ligand (DPPZ-Si), its complex and precursors.

3.5.3 Fluorescence Spectroscopy Studies

The free DPPZ-Si ligand (Figure 34) displayed a fluorescence maximum at around 440 nm (λ_{ex}= 349 nm) while emitting over a range from ~ 375-625 nm.

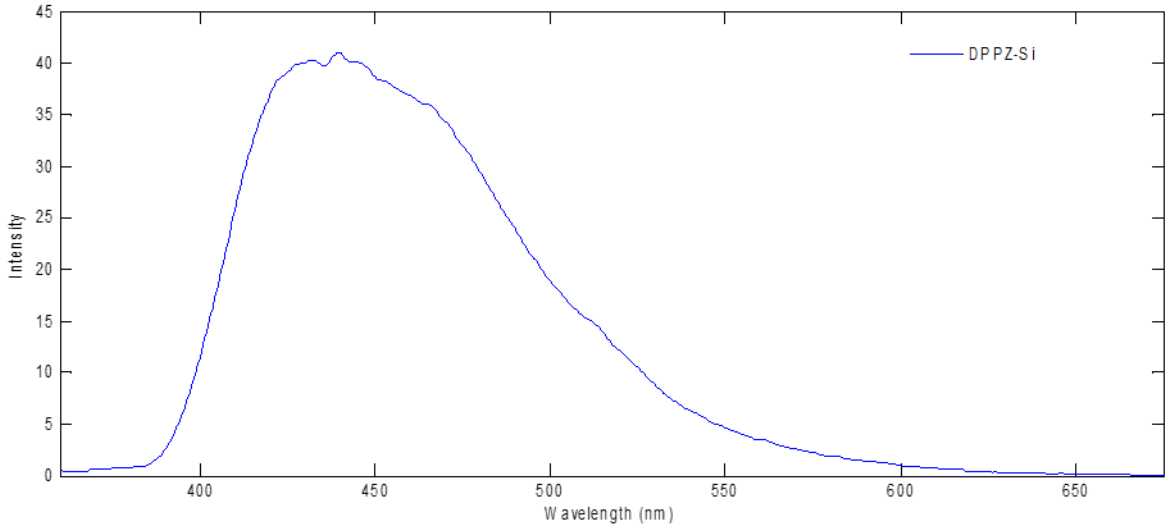

Figure 34. Fluorescence spectrum for the free ligand DPPZ-Si.

Fluorescence spectrum for the $Eu(tta)_3DPPZ\text{-}Si$ complex (Figure 35) were measured with 347 nm as the excitation wavelength shows the presence of two emissive states. The narrow peaks observed in the spectra are the transitions between the $^5D_0$ excited state of Eu^{3+} and the different J levels of the ground term ^7F (^7F_J=0-3).

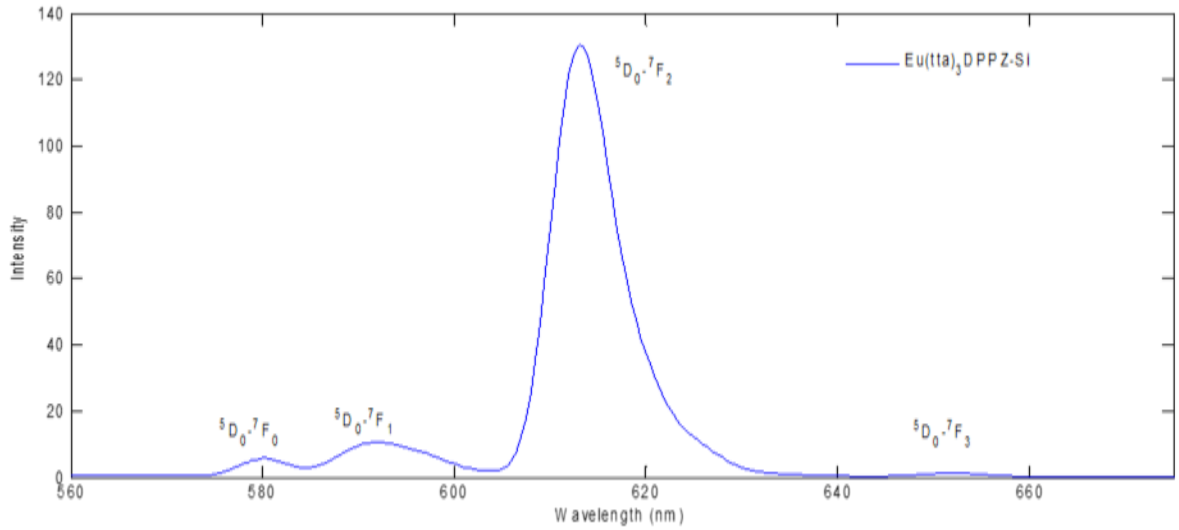

Figure 35. Emissive state transitions for $Eu(tta)_3DPPZ\text{-}Si$.

The $^5D_0$-$^7F_2$ transition at λ=613 nm exhibits the strongest emission due to its induced electric dipole transition from its highly polarizable environment around the Eu^{3+} ion. This is emission is responsible for the bright red luminescence imparted by Eu^{3+} complexes. The intensity of the $^5D_0$-$^7F_1$ transition at λ=592 nm is significantly weaker than that of the $^5D_0$-$^7F_2$ transition due to its independence of the coordination environment as well as primarily being a magnetically induced transition. The $^5D_0$-$^7F_0$ (λ=580) and $^5D_0$-$^7F_3$ (λ=652) are even weaker than the $^5D_0$-$^7F_1$ transition due to their inability to induce a magnetic or electric dipole transition.

While the broad emission ranging from 375 nm to 550 nm originates from energy absorbed by the DPPZ-Si ligand in the complex as observed in Figure 34. When in comparison to the complex fluorescence spectra, the DPPZ-Si ligand weak emission was able to transfer

more energy to the Eu(III) ion than $Eu(tta)_3DPPZ\text{-}CH_3$ and $Eu(tta)_3DPPZ\text{-}COOH$, but less than $Eu(tta)_3DPPZ\text{-}COOEt$ and $Eu(tta)_3DPPZ$, which is indicative of a lower triplet energy state than that of europium. No transitions starting from the $^5D_1$ state were observed for this complex.

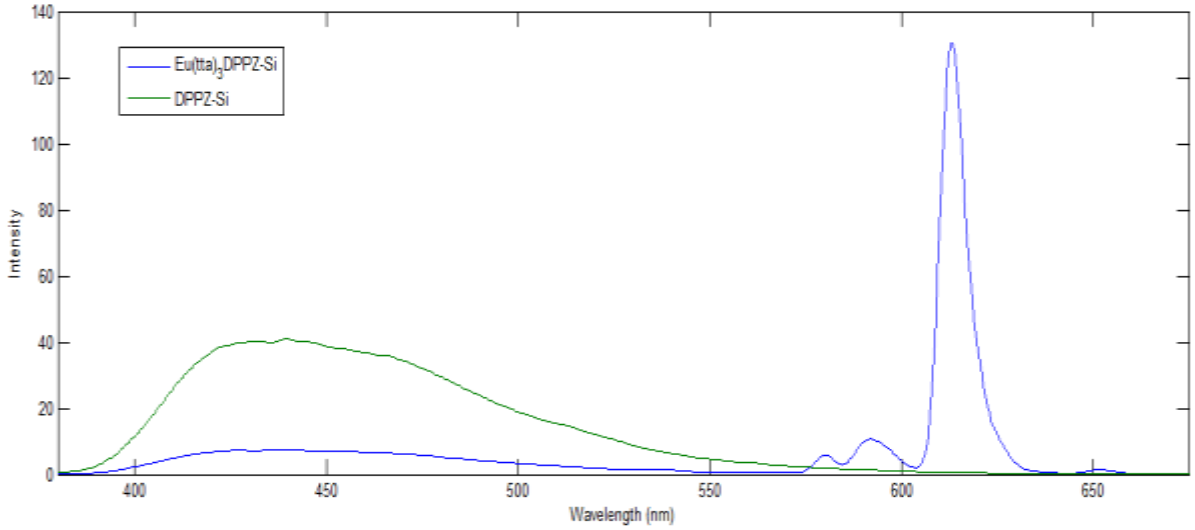

Figure 36. Fluorescence Spectra ofDPPZ-Si and $Eu(tta)_3DPPZ$-Si.

The addition of TEOS, ethanol, ammonium hydroxide (28% NH_4OH) and water to $Eu(tta)_3DPPZ$-Si in the formation of the silica nanoparticle exhibited no induced magnetic or electric dipole transitions characteristic of Eu^{3+} complexes. There are multiple factors that could contribute to the inefficiency of the nanoparticle. Under the conditions of base catalysis large sol-gel particles are believed to have formed, thus leading to light scattering occurring as indicated by the IR spectrum in Figure 32.

To decrease the size of the nanoparticle, the amount of $Eu(tta)_3DPPZ$-Si added was increased from 20 mg to 50 mg. To correct for the possibility of light scattering a solvent (DMSO, n=1.479) with a similar refractive index to that of the silica matrix in a silica nanoparticle (n=1.475) was used instead of water (n=1.333). Neither solution resulted in transitions characteristic of Eu^{3+} complexes.

Other factors possibly contributing to the lack of emission by the silica nanoparticle include: fluorescence quenching by unbound $Eu(tta)_3$DPPZ-Si encased inside the nanoparticle, and an inefficient silane coupling agent.

3.6 Comparison of the UV-Vis and Fluorescence Measurements of the Ligands and Eu^{3+} Complexes

The unfunctionalized DPPZ ligand was the basis for which the variations in the electronic properties of the other functionalized DPPZ ligands were determined. DPPZ gives us a baseline from which to discern a relationship upon the substitution of either electron donating or withdrawing functional groups to the ligand. As discussed earlier, DPPZ exhibits absorption events at 268, 359, and 378 nm. Upon the substitution of an electron donating methyl group to the DPPZ ligand (DPPZ-CH_3), a red shift to 273, 367, and 387 nm occurs. With the substitution of electron withdrawing groups (-COOEt, -Si, -COOH) to the DPPZ ligand, a red shift also occurs for DPPZ-COOEt (277, 366, and 386nm), DPPZ-Si (269, 367, and 385 nm) and DPPZ-COOH (275, 369, and 388 nm). The UV-Vis spectra for the ligands (Figure 37) showed that both the electron donating and electron withdrawing groups experienced a red shift in comparison to DPPZ.[28]

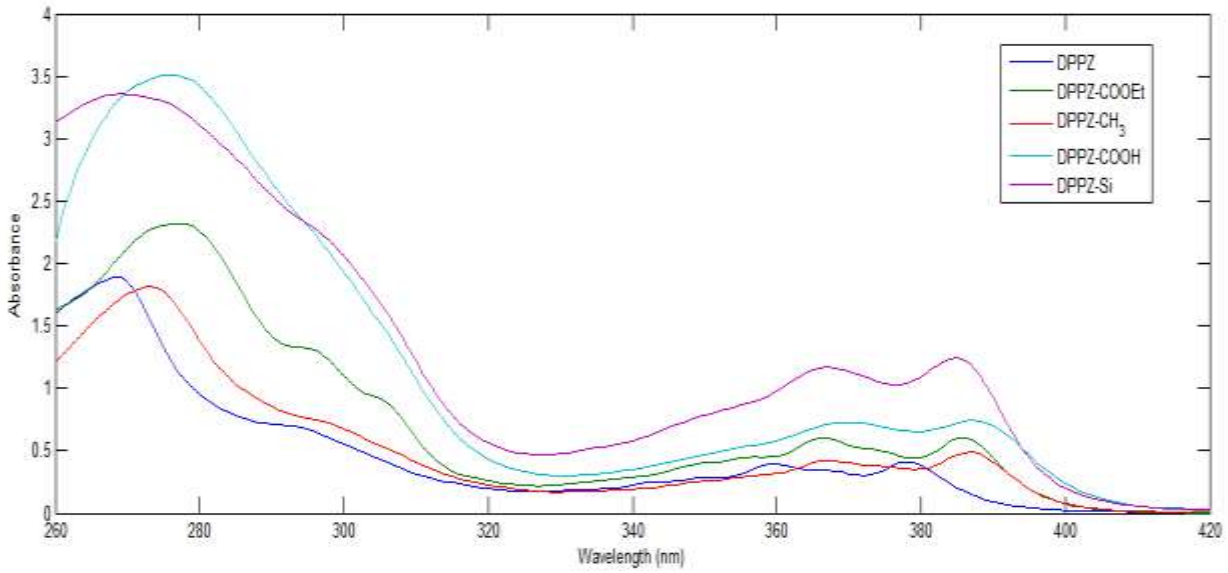

Figure 37. UV-Vis spectra of the various DPPZ ligands.

Upon complexation, the $Eu(tta)_3DPPZ$ complex served as the basis for which the variations in the electronic properties of the other coordination complexes were determined. $Eu(tta)_3DPPZ$ exhibit absorption events at 272, 341, 356, and 375 nm. The band gap between the highest occupied molecular orbital (HOMO) and the lowest unoccupied molecular orbital (LUMO) is expected to narrow in the presence of an electron withdrawing substituent which would result in a red shift to lower energies (higher wavelengths). The electron withdrawing substituted complexes all exhibited red shifts when compared to $Eu(tta)_3DPPZ$. $Eu(tta)_3DPPZ$-COOEt (275, 346, 363, 383 nm), $Eu(tta)_3DPPZ$-Si (279, 346, 363, 382 nm), and $Eu(tta)_3DPPZ$-COOH (273, 346, 369, 388 nm).[28]

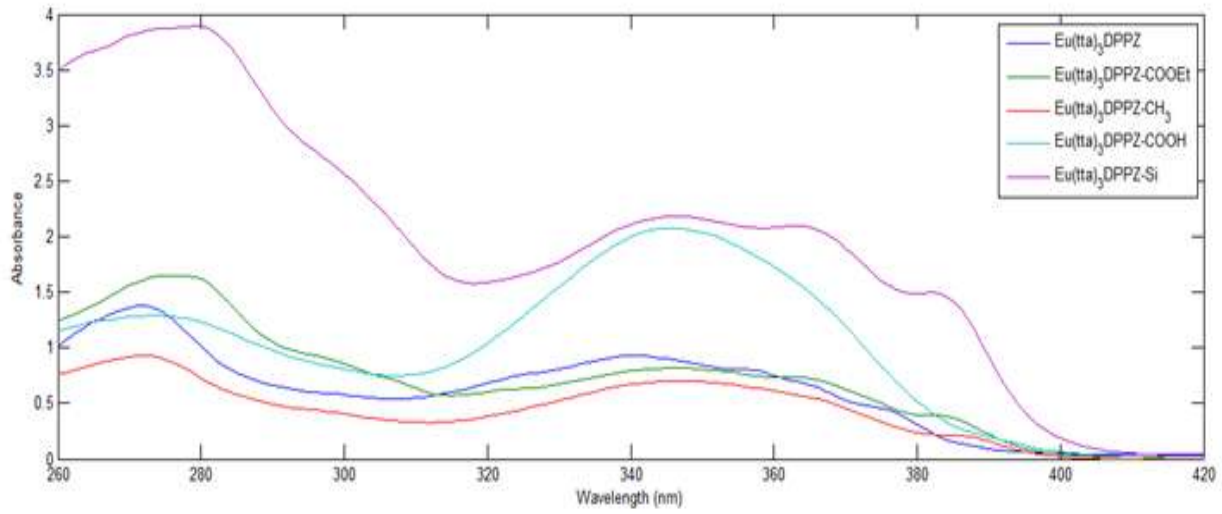

Figure 38. Various UV-Vis spectra of $Eu(tta)_3DPPZ$ complexes.

It was believed that the electron donating $Eu(tta)_3DPPZ\text{-}CH_3$ complex would experience a higher band gap (higher energy = lower wavelengths) due to the methyl substituent switching the LUMO character to that of tta π^* orbitals, but it exhibited a red shift like all of the other complexes (Figure 38) did which is indicative of maintaining its respective π^* orbitals.

From the UV-Vis measurements, along with trial and error, the excitation wavelength for the fluorescence measurements were determined to be at various wavelengths in the 340 nm region for all of the complexes. The most efficient excitation energy for the fluorescence measurements in the 340 nm region correspond to the absorption events associated with tta. This is indicative of the S1 state for most of the complexes being inhabited as a result of the promotion of an electron from tta based π orbitals to DPPZ based π^* orbitals via ligand-to-ligand charge transfer. This also corresponds to the red shifts in the absorptions observed for the electron withdrawing ligands and complexes. The efficiency of intersystem crossing (ISC) and energy transfer (ET) is essential in achieving a complex with a good quantum yield. The electron withdrawing complexes ($Eu(tta)_3DPPZ\text{-}COOEt$, $Eu(tta)_3DPPZ\text{-}Si$, and $Eu(tta)_3DPPZ\text{-}Si$) inability to adequately sensitize the Eu (III) ion can be attributed to their lower triplet state

energy not being able to transfer energy to the $^5D_0$ level efficiently which is why they experience a dramatically decreased quantum yield with respect to Eu(tta)$_3$DPPZ. The electron donating complex (Eu(tta)$_3$DPPZ-CH_3), being the least efficient, must have a high intersystem crossing value (more energy required) as well as a lower triplet energy state in order to explain its decrease in quantum yield when compared to Eu(tta)$_3$DPPZ. Figure 39 shows how efficient each ligand was at transferring energy to the Eu (III) ion. Eu(tta)$_3$DPPZ-CH_3 transferred the least amount of energy to the $^5D_0$-$^7F_2$ centered emission for europium based off the ligands retention of energy, with more intense emissions originating from the $^5D_1$ and $^5D_0$-$^7F_1$ transitions explaining why its quantum yield was the lowest among all of the other complexes. While the electron withdrawing groups were able to transfer similar amounts of energy to the Eu (III) ion, Eu(tta)$_3$DPPZ-COOH had minimal energy to transfer from the ligand to begin with, transferred the second least amount of energy to the Eu (III) ion. With more intense emissions originating from the $^5D_1$ and $^5D_0$-$^7F_1$ transitions explaining why its quantum yield was the second lowest among all of the other complexes. Eu(tta)3DPPZ-Si and Eu(tta)3DPPZ-COOEt transferred almost identical amounts of energy to the complex (according to their residual ligand emissions), but Eu(tta)$_3$DPPZ-COOEt was able to transfer more energy to the $^5D_0$-$^7F_2$ centered transition than Eu(tta)$_3$DPPZ-Si. Thus making them the second and third most efficient complexes respectively. Eu(tta)$_3$DPPZ was able to transfer the most energy to the $^5D_0$-$^7F_2$ centered transition compared to the rest of the complexes which explains why it was the most efficient complex, giving it the highest quantum yield.

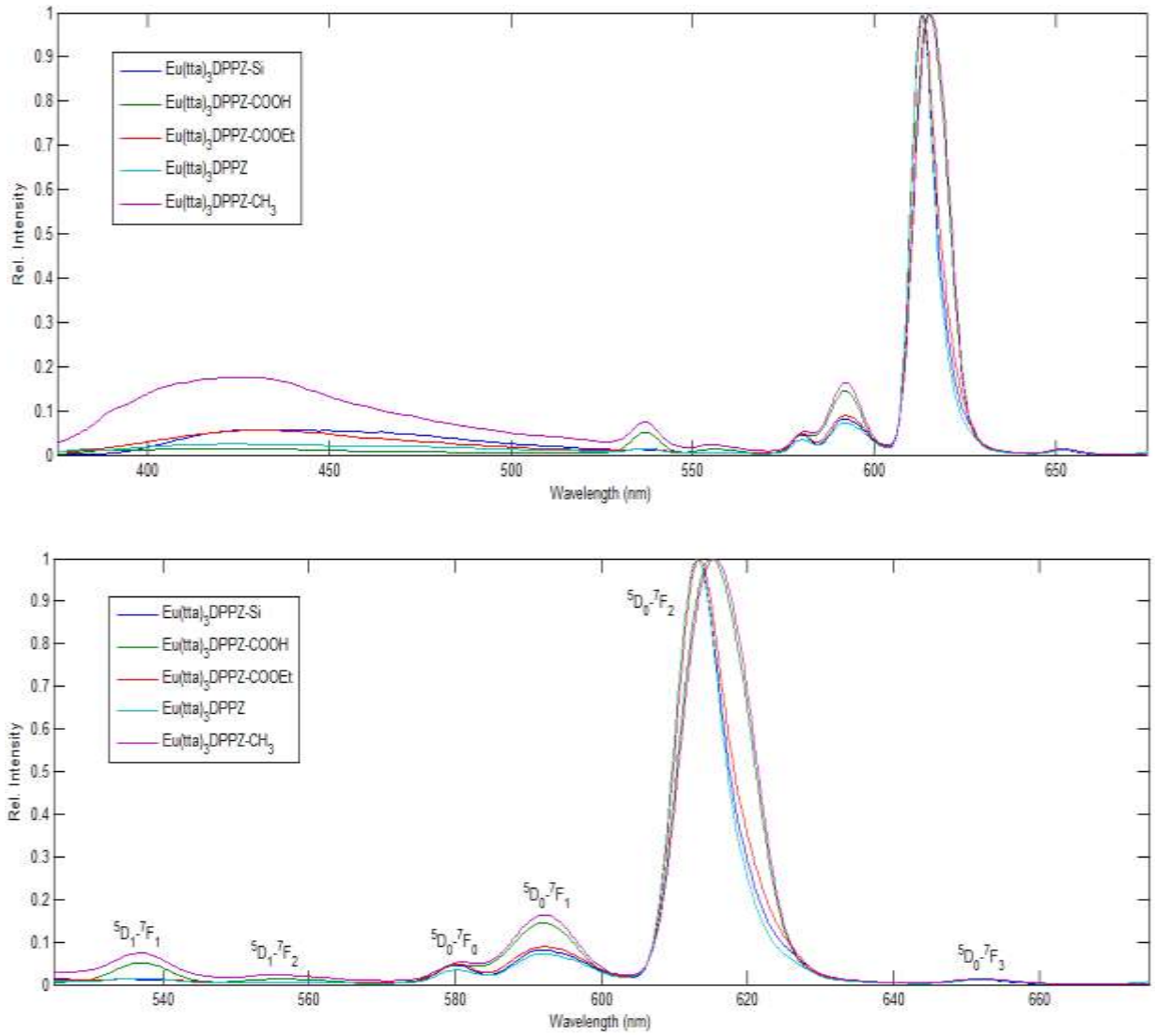

Figure 39. Various $Eu(tta)_3DPPZ$ functionalized complexes fluorescence spectra.

3.7 Quantum Yield Calculations

For the Eu^{3+} complexes a variety of solvents were utilized. $Eu(tta)_3DPPZ$, $Eu(tta)_3DPPZ$-CH_3/$Eu(tta)_3DPPZ$-COOH, and $Eu(tta)_3DPPZ$-COOEt/$Eu(tta)_3DPPZ$-Si measurements were made in acetonitrile (n=1.3441), DMSO (n=1.4793), and chloroform (n=1.4458) respectively. The excitation wavelength ranges from 342-349 for the various complexes, while the emission range used to calculate the integrated fluorescence intensity for the complexes was from 550-664 nm. Baseline absorption and emission spectra of pure solvents were also collected (at their

respective excitation wavelengths) to be subtracted from the measured absorption and emission spectra to correct for background absorption or emission imparted by the solvents. Table 1 summarizes the values used (after correction) as well as the quantum yields for each complex.

Table 1: Summary of quantum yield calculations and values used for Eu^{3+} complexes.

Complex	$\lambda_{exc.}$ (nm)	Abs.	I	Abs.Ref.	I Ref.	n	n Ref.	QY Ref.	QY (%)
$Eu(tta)_3DPPZ$	342	0.073802	3732.718	0.06006	21608.99	1.3441	1.3284	0.54	7.68±0.06
$Eu(tta)_3DPPZ\text{-}CH_3$	349	0.081592	290.4587	0.06006	21608.99	1.4793	1.3284	0.54	0.59±0.02
$Eu(tta)_3DPPZ\text{-}COOEt$	347	0.096549	616.373	0.06006	21608.99	1.4458	1.3284	0.54	1.04±0.05
$Eu(tta)_3DPPZ\text{-}COOH$	349	0.049836	180.5463	0.06006	21608.99	1.4793	1.3284	0.54	0.61±0.07
$Eu(tta)_3DPPZ\text{-}Si$	347	0.093714	375.5567	0.06006	21608.99	1.4458	1.3284	0.54	0.65±0.04

The results show that the complex capable of more efficient ligand to metal energy transfer was the un-functionalized DPPZ complex ($Eu(tta)_3DPPZ$). Based on the complexes quantum yield value (7.68 %), it was the most efficient out of the complexes observed due to its HOMO being primarily tta π^* in nature allowing for more efficient ligand-to-ligand transfer of energy.[28] Upon substitution of DPPZ with electron withdrawing functional groups (-COOEt, -Si, -COOH), as well as the electron donating group ($-CH_3$), a significant decrease in quantum yield was observed. $Eu(tta)_3DPPZ\text{-}COOEt$ was found to be the second most efficient complex based off of its quantum yield (1.04 %). These two complexes were the only ones found to have a quantum yield higher than that of $Eu(tta)_3(H_2O)_2$ (0.73 %). While $Eu(tta)_3DPPZ\text{-}Si$ (0.65 %), $Eu(tta)_3DPPZ\text{-}COOH$ (0.61 %) and $Eu(tta)_3DPPZ\text{-}CH_3$ (0.59 %) all experienced a similar decrease in quantum yield which showed a diminished quantum yield from that of the dihydrate species. The decrease in quantum yield for the electron withdrawing complexes can be attributed to lower triplet energy states than that of the Eu (III) ion leading to an inefficient transfer of energy from the ligand to the metal ion. The electron donating complex ($Eu(tta)_3DPPZ\text{-}CH_3$), being the least efficient, must have a high intersystem crossing value (more energy required) as

well as a lower triplet energy state in order to explain its decrease in quantum yield when compared to $Eu(tta)_3DPPZ$.[28] Another factor possibly causing the decrease in quantum yield for all of the complexes could be due to either C-H ($Eu(tta)_3DPPZ$-COOEt, $Eu(tta)_3DPPZ$-Si, $Eu(tta)_3DPPZ-CH_3$), N-H (Eu(tta)3DPPZ-Si), or O-H ($Eu(tta)_3DPPZ$-COOH) oscillators being in close proximity to the Eu^{3+} metal center which quenches the luminescence via a vibrational (non-radiative) relaxation pathway.[2] Other factors possibly affecting the ability of the ligands to efficiently transfer energy to the Eu^{3+} ion could be the polarity of the solvents, either via hydrogen bonding, direct intermolecular bonding (excited species) or dipole-dipole interactions with the ligand

3.8 Conclusion

In this project, the luminescence properties of dipyridophenazine precursors and their respective Eu^{3+} complexes, as well as one of the complexes ($Eu(tta)_3DPPZ$-Si) encased into the silica matrix of a nanoparticle were probed to determine the efficiency of ligand to metal energy transfer while exploring the effect different electron withdrawing or donating functional groups had on the quantum yield of the complexes. The ligands were characterized using different spectroscopic techniques to confirm their structure and functionalization. The complexes optical properties were calculated from absorption and fluorescence measurements.

It was believed that the substitution of solvent molecules from $Eu(tta)_3(H_2O)_2$ with the bidentate nitrogen ligands of the functionalized and un-functionalized DPPZ ligands would lead to an increase in luminescence quantum yields. Furthermore, it was believed that the variation in complex luminescence upon substituent substitution of the ligand would increase with electron donating groups, and decrease with electron withdrawing groups. The unfunctionalized complex, Eu(tta)3DPPZ, exhibited the highest quantum yield value (Q.Y.= 7.68 %). It was the

most efficient out of the complexes observed due to its HOMO being primarily tta π^* in nature allowing for more efficient ligand-to-ligand transfer of energy.[28] The data confirmed a significant decrease in quantum yield upon the addition of electron withdrawing groups in $Eu(tta)_3DPPZ$-COOEt (Q.Y.= 1.04 %), $Eu(tta)_3DPPZ$-Si (Q.Y.= 0.65 %), and $Eu(tta)_3DPPZ$-COOH (Q.Y.= 0.61 %) which was attributed to the complexes having lower triplet state energies not being able to transfer energy to the $^5D_0$ level of the Eu (III) ion efficiently. However, the addition of the electron donating methyl group in $Eu(tta)_3DPPZ$-CH_3 (Q.Y.= 0.59) did not exhibit an increase in quantum yield as expected, but was instead the least efficient of all the complexes observed due to a lower energy state and a high intersystem crossing value . In conclusion, the un-functionalized DPPZ complex, $Eu(tta)_3DPPZ$, was the only complex to show enhanced luminescent properties capable of potential applications in biomedical imaging.

3.9 Future Work

In continuing this work, a crystallographic and computational study should be conducted in order to verify the structural data and better investigate the energy transfer process between the ligands (tta and functionalized DPPZ complexes), and the metal center ion (Eu^{3+}). The molecular data acquired from the crystallographic study could determine if site to site inhomogeneities are causing luminescence quenching or not, while a computational study will help better determine which functional groups will tune the DPPZ ligand energy levels to where they are more conducive to efficient energy transfer to the Eu^{3+} ion. Substitution of complexes containing C-H, N-H, O-H oscillators with more conducive energy transfer groups (aromatic, trifluorene, etc) could be probed to see if there is an increase in quantum yield or not.

Also, future studies should account for potential quenching effects due to solvent interaction with the complexes. Complexes optical properties should be characterized using

various polar and non-polar solvents to determine whether or not there are significant changes in the absorption or emission spectra. In doing a solvent polarity study, one could also use a deuterated solvent to ensure that there is no luminescence quenching due to hydrogen bonding between to solvent and complexes during the excitation process.

For future silica nanoparticle synthesis and characterization, since acidic catalysis could lead to a dissociation of the Eu^{3+} β-diketonate complex and protonation of the phenantroline portion of the DPPZ ligand and basic catalysis lead to the development of large sol-gel particles, it is suggested that either further permeations of the DPPZ-Si:APTS:TEOS:H_2O and base concentration be explored or a neutral pH method be implemented to achieve a successful sol-gel composition capable of luminescing. A different silane coupling agent should also be probed due to the low quantum yield of the Eu(tta)3DPPZ-Si complex. Dipodal silanes could be an interesting substitute due to their impact on substrate bonding (capable of six bonds instead of three) and hydrolytic stability.

REFERENCES

1. Ma, Y.; Wang Y. Recent advances in the sensitized luminescence of organic europium complexes. *Coordin. Chem. Rev.* **2010**, 254, 972–990.

2. Li, J.; Li, H.; Yan P.; Chen, P.; Hou, G.; Li, G. Synthesis, crystal Structure, and luminescent properties of 2-(2,2,2-trifluoroethyl)-1-indone lanthanide complexes. *Inorg. Chem*. **2012,** 51(9), 5050-7.

3. Mihailovic, A.; Vladescu, I.; McCauley, M.; Ly, E.; Williams, M.C.; Spain, E.M.; Nuñez, M.E. Exploring the interaction of ruthenium(II) polypyridyl complexes with DNA using single-molecule techniques. *Langmuir***. 2006**, 22(10), 4699-4709.

4. Divya, V.; Sankar, V.; Raghu, K.G.; Reddy, M.L.P. A mitochondria-specific visible-light sensitized europium β-diketonate complex with red emission. *Dalton T*. **2013**, 42, 12317.

5. De Silva, C.R.; Maeyer, J.R.; Wang, R.; Nichol, G.S.; Zheng, Z. Adducts of europium b-diketonates with nitrogen p,p^{0}-disubstituted bipyridine and phenanthroline ligands: synthesis, structural characterization, and luminescence studies. *Inorg. Chim. Acta*. **2007**, 360, 3543–3552.

6. Handl, H.L.; Gillies' R.J. Lanthanide-based luminescent assays for ligand-receptor interactions. *Life Sci*. **2005**, 77, 361–371.

7. Liu, H.K.; Sadler, P.J. Metal Complexes as DNA Intercalators. *Accounts Chem. Res.* **2011**, 44(5), 349-59.

8. Roark, K.; Dinkelmeyer, B, Synthesis of 1,10-phenanthroline-5,6-dione, dipyrido[3,2-a:2',3'-c]phenazine (dppz), and 1,10-phenanthroline-3,4-diaminotoluene; *Chem. 380 Research Project*, Western Carolina University, Cullowhee; p. 1, 2, 4.

9. Shao, F.; Elias, B.; Lu, W.; Barton, J.K. Synthesis and characterization of iridium(III) cyclometalated complexes with oligonucleotides: insights into redox reactions with dna. *Inorg. Chem.* **2007**, 46, 10187-10199.

10. Ossipov, D.; Zamaratski, E.; Chattopadhyaya, J. Synthesis of dipyrido[3,2-a:2',3'-c]phenazine-11-carboxylic acid. Dipyrido[3,2-a:2',3'-c]phenazine-tethered oligo-dna: synthesis and thermal stability of their dna-dna and dna-rna duplexes and dna-dna-dna triplexes. *Helv. Chim. Acta*. **1999**, 82, 2195.

11. Wu, X.; Cong, Y.; Liu, Y. Luminescence and oxygen sensing properties of ORMOSILs covalently grafted with novel ruthenium(II) complex. *J. Sol-Gel Sci. Technol*. **2009**, 49, 355-363.

12. Binnemans, K.; Lenaerts, P.; Driesen, K.; Gorller-Walrand, C. A luminescent tris(2-thenoyltrifluoroacetonato) europium(III) complex covalently linked 1,10-phenanthroline-functionalized sol-gel glass. *J. Mater. Chem*. **2004**, 191-195.

13. Lundin, N.; Walsh, P.; Howell, S.; McGarvey, J.; Blackman, A.; Gordon, K. Complexes of Functionalized Dipyrido[3,2-a:2',3'-c]-phenazine: A Synthetic, Spectroscopic, Structural, and Density Functional Theory Study. *Inorg. Chem*. **2005**, 44, 3551-3560.

14. Li, H.R.; Lin, J.; Zhang, H.J.; Li, H.C.; Fu, L.S.; Meng, Q.C. Novel covalently bonded hybrid materials of europium (terbium) complexes with silica. *Chem. Commun*. **2001**, 1212-1213.

15. Nassar, E.J.; Ciuffi, K.J.; Lima Ribiero, S.J.; Messaddeq, Y. Europium Incorporated in Silica Matrix Obtained by Sol-Gel: Luminescent Materials. *Materials Research*. **2003**, 6(4), 557-562.

16. Wolkenberg, S.E.; et al. Design, synthesis, and evaluation of novel 3,6-diaryl-4-aminoalkoxyquinolines as selective agonists of somatostatin receptor subtype 2. *J. Med. Chem*. **2011**, 54(7), 2351-2358.

17. Guangbo, C.; Welian, L.; Kong, Z.; Su, Z.; Chu, B.; Li, B.; Zhang, Z.; Hu, Z.; Chi, H. Hydrothermal Syntheses of Some Derviatives of Tetraazatiphenylene. *Synth. Commun*. **2006,** 36, 2519-2524.

18. Shi, J.; Hou, Y.; Chu, W.; Shi, X.; Gu, H.; Wang, B.; Sun, Z. Crystal Structure and Highly Luminescent Properties Studies of Bis-β-diketonate Lanthanide Complexes. *Inorg. Chem*. **2013**, 52, 5013-5022.

19. Hou, Y.; Shi, J.; Chu, W.; Sun, Z. Synthesis, Cyrstal Structure and Near-IR Luminescent Properties of Lanthanide Bis(β-diketonate) Complexes. *Eur. J. Inorg. Chem*. **2013**, 3063-3069.

20. Franville, A-C.; Zambon, D.; Mahiou, R. Luminescence Behavior of Sol-Gel Derived Hybrid Materials Resulting from Covalent Grafting of Chromophore Unit to Different Organically Modified Alkoxysilanes. *Chem. Mater*. **2000**, 12, 428-435.

21. Wong, K.; Law, G.; Murphy, M.; Tanner, P.; Wong, W.; Kwan-Sing Lam, P.; Hon-Wah Lam, M. Functionalized Europium Nanorods for In Vitro Imaging. *Inorg. Chem*. **2008**, 47, 5190-5196.

22. Lopez, R.; Moya, S.A.; Zu´niga, C.; Ya´nez, M.; Bayon´, J.C.; Aguirre, P. Design and spectroscopic study of new ruthenium(II) complexes containing ligands derived from terpyridine and dipyrido[3,2-a:2,3-c]phenazine: {Ru(4-Rph-tpy) [dppz(COOH)]Cl}PF6 with R = NO2, Br, Cl.

23. Christopher R. Treadway's Dissertation Project at Cal Tech (Spectroscopic Characterization of DNA Mediated Charge Transfer): http://thesis.library.caltech.edu/2038/1/00Title_Page.pdf.

24. Gelest. Silane Coupling Agents: Connecting Across Boundaries. http://www.gelest.com/goods/pdf/couplingagents.pdf.

25. Fluor Tools. UV-Vis-IR Spectral Software: Calculate fluorescence quantum yield. http://www.fluortools.com/software/ae/documentation/qy.

26. UC Davis ChemWiki; Electronic Spectroscopy: Interpretation. http://chemwiki.ucdavis.edu/Physical_Chemistry/Spectroscopy/Electronic_Spectroscopy/Electronic_Spectroscopy%3A_Interpretation.

27. Zheng, Y.; Zhou, Y.; Yu, J.; Yu Y.; Zhang, H.;Gillin W.P.. Electroluminescence from $^5D_0 \rightarrow {}^7F_J$ and $^5D_1 \rightarrow {}^7F_J$($J$=0-4) transitions with a europium complex as emitter. *J. Phys. D: Appl. Phys*. **2004**, 37, 531–534.

28. Nolasco, M.; Vaz, P.; Carlos, L. The role of 4,7-disubstituted phenantrholine ligands in energy transfer europium (III) complexes: a DFT study. *New J. Chem*. **2011**, 35, 2435-2441.

SUPPLEMENTARY MATERIAL

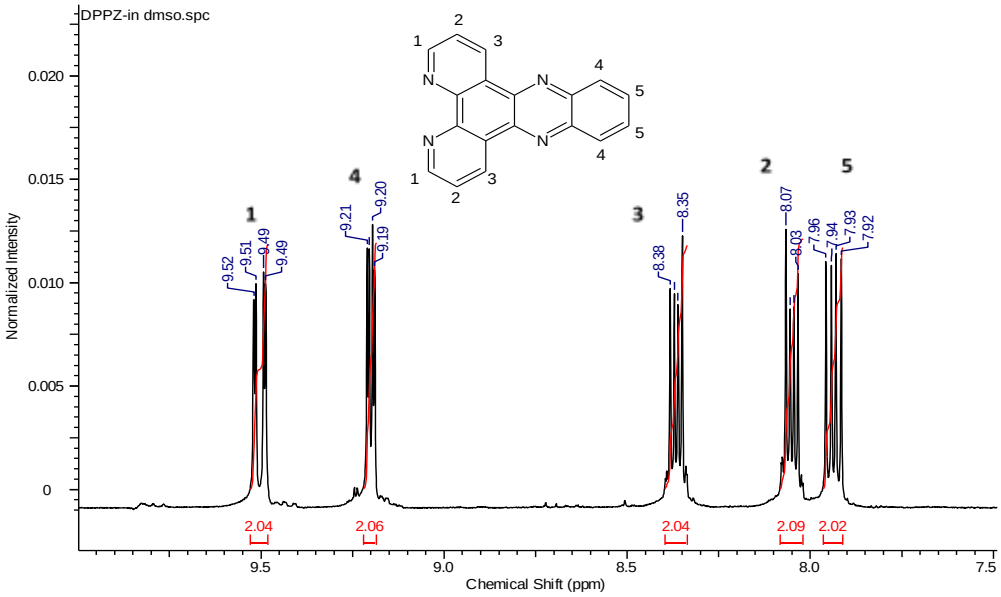

S 1. NMR spectra for DPPZ,

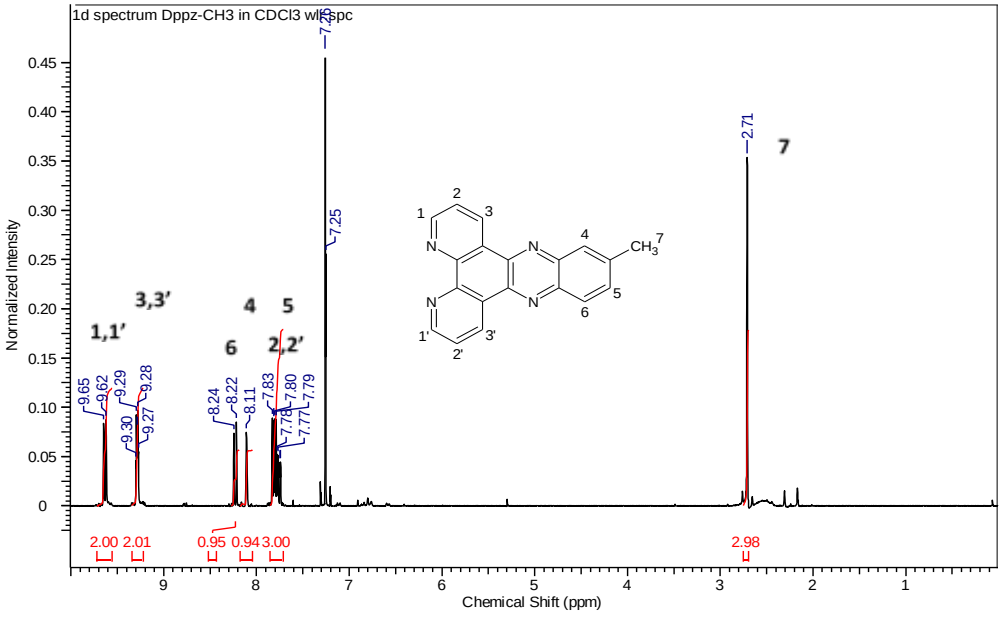

S 2. NMR Spectra for DPPZ-CH_3.

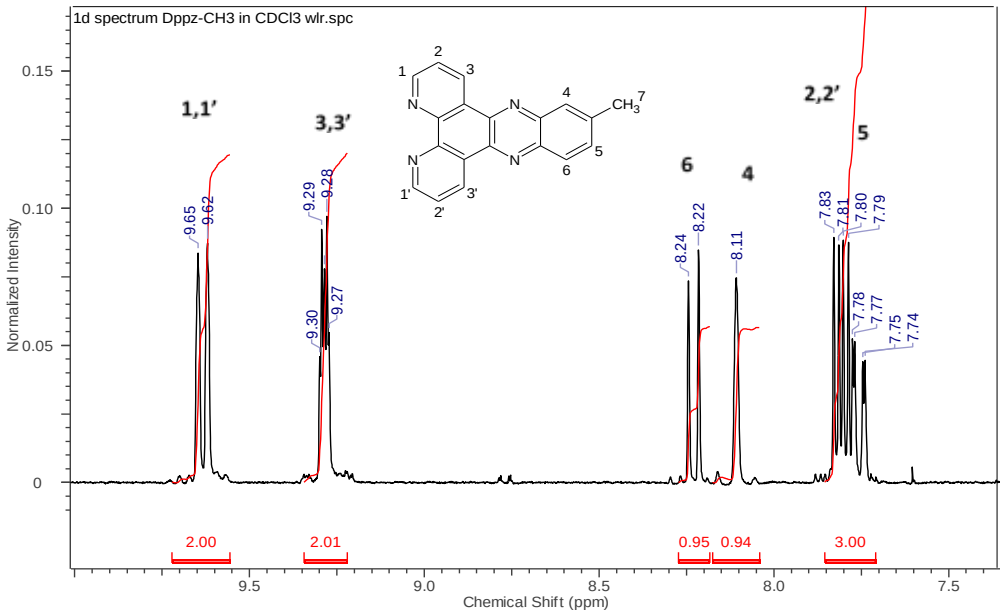

S 3. NMR Spectra for DPPZ-CH_3.

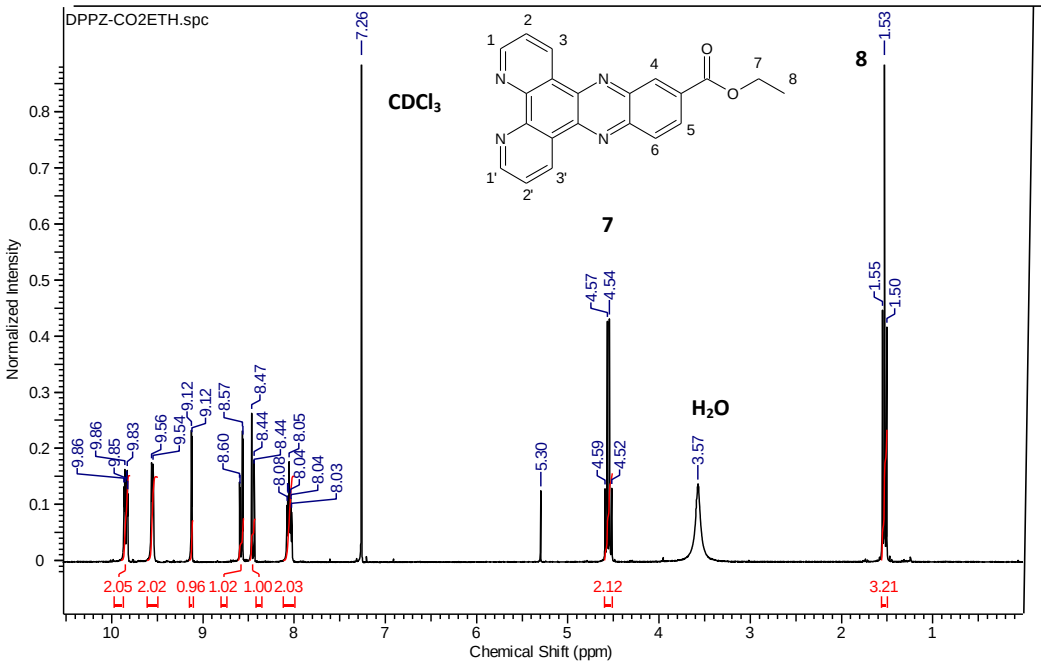

S 4. NMR Spectra for DPPZ-COOEt.

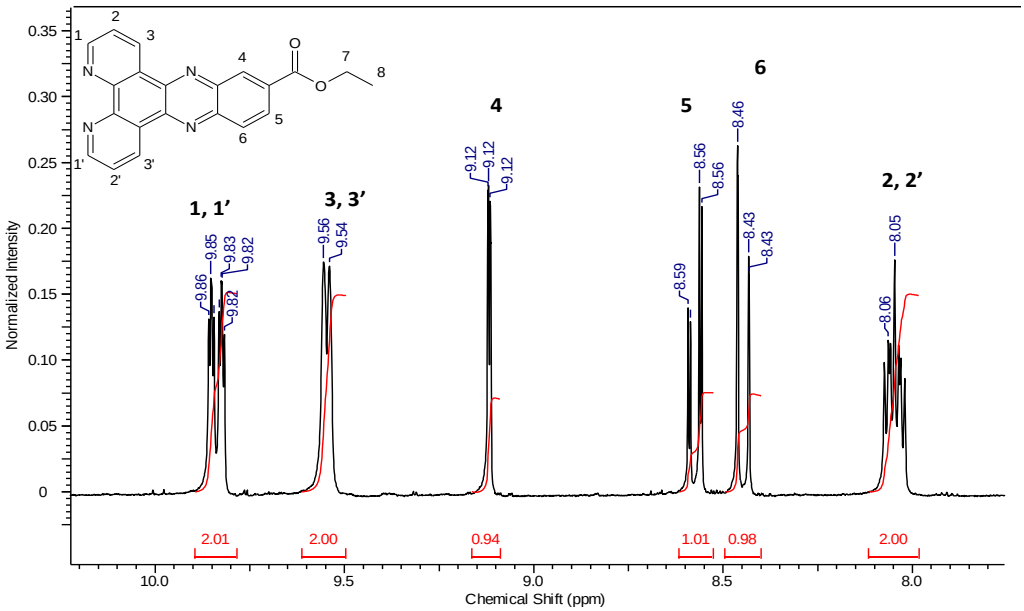

S 5. NMR Spectra for DPPZ-COOEt.

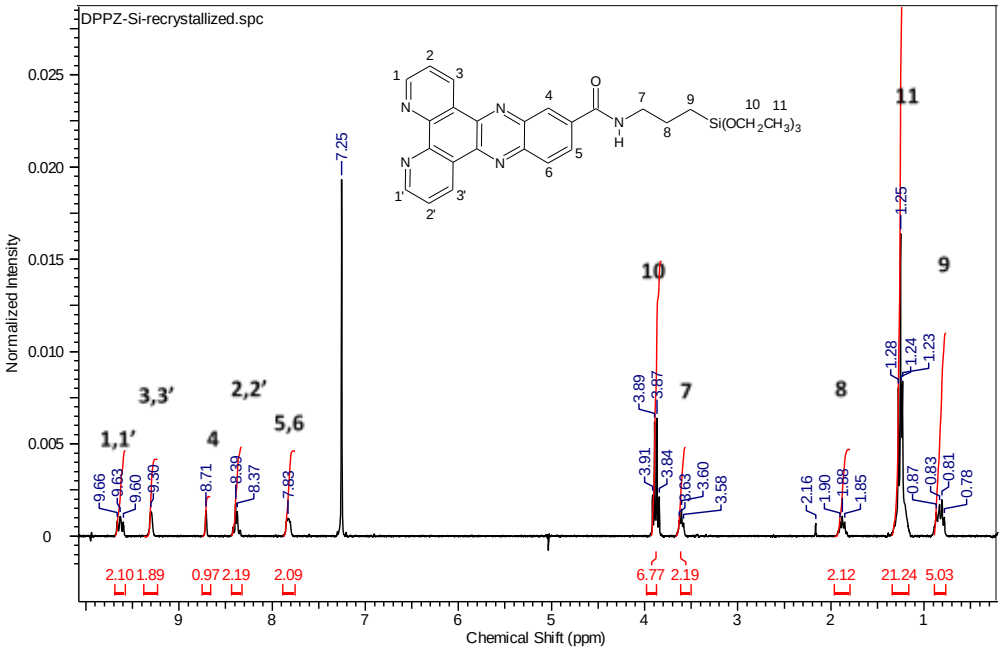

S 6. NMR Spectra for DPPZ-Si.

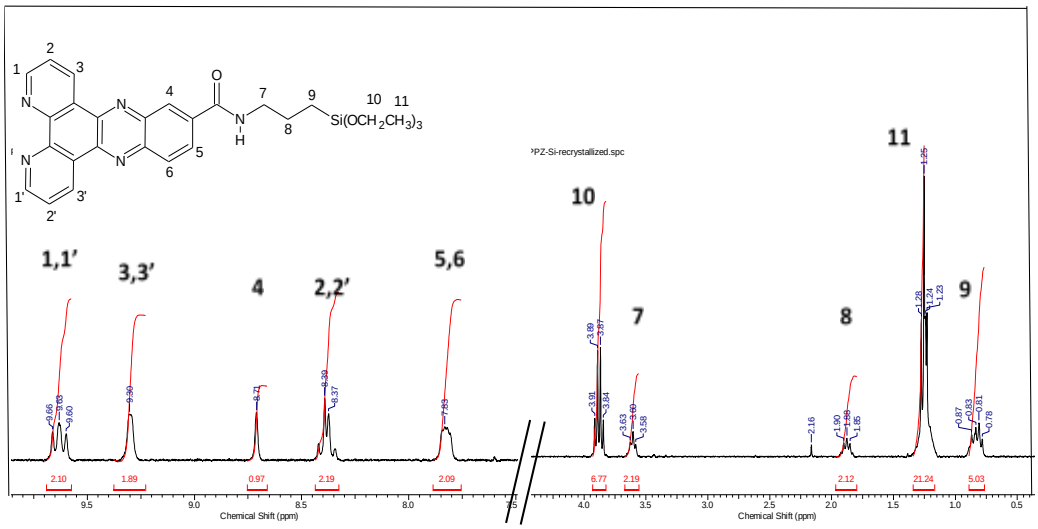

S 7. NMR Spectra for DPPZ-Si

.

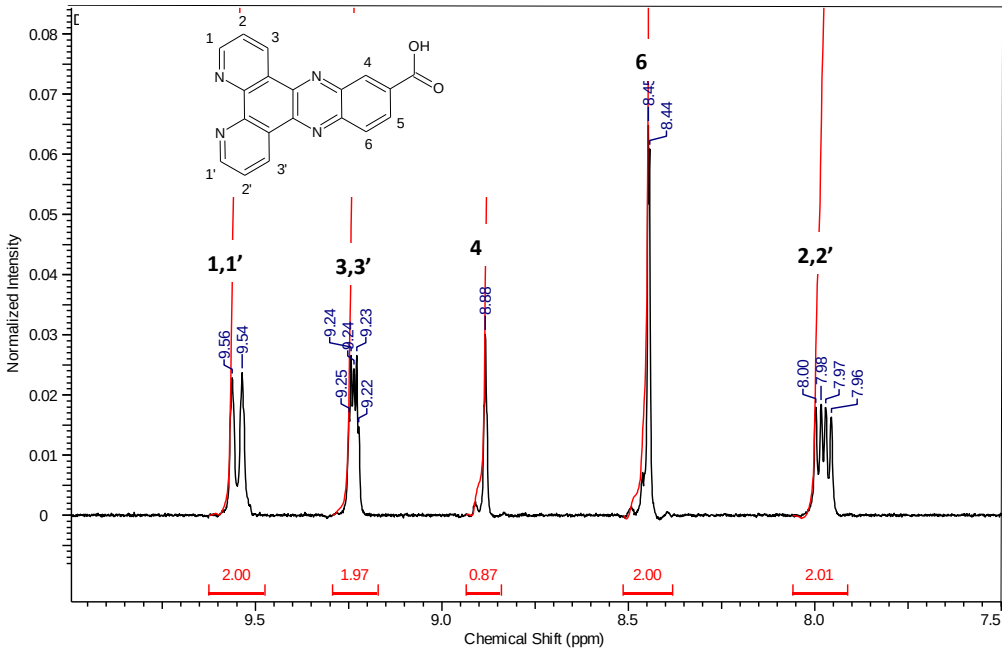

S 8. NMR Spectra for DPPZ-COOH.